University of Stavanger

Faculty of Science and Technology

MASTER'S THESIS

Study program/ Specialization: Offshore Technology / Subsea Technology	Spring semester, 2016 Open / ~~Restricted~~ access
Writer: Artem Yastrebov	.... (Writer's signature)
Faculty supervisor: Ole-Erik Vestøl Endrerud **External supervisor:** Tommy Svartvatn (E Plug AS)	
Thesis title: Vibration energy harvesting in a well	
Credits (ECTS): 30	
Key words: energy harvesting, vibrations, autonomous devices, B-annulus	Pages: ……… IX + 44 ……… + enclosure: …… 11 ……… Stavanger, 15 June 2016 Date/year

Abstract

The main objective of this thesis is to study the possible solution for the supply of electric energy to autonomous systems in a well via vibration harvesting modules.

Some autonomous systems such as pressure/temperature sensors located for example in the B-annulus, should be powered in order to function. This represents a significant challenge in in subsea wells, since penetrations in subsea wellheads are not allowed by the current standards [1]. One of the solutions to the power supply challenge is to use energy harvesting modules. Since during drilling and production phases multiple sources of vibrations are present these modules can potentially be used. The use of vibration harvesting modules for powering autonomous sensors in inaccessible locations can potentially decrease complexity of monitoring systems, significantly reduce installation time and costs.

In order to identify to what extend the vibration harvesting module can be used for the power supply an experiment of using the Vibration Harvesting Module (VHM) is performed. The experiment setup which was used to estimate certain parameters of the vibration harvesting module, calculations justifying the choice of equipment and experimental procedure are provided in the thesis. The experiments consisted of three parts: two experiments with induced vibrations by using two different vibration motors and one experiment with natural oscillations. It was concluded that natural oscillations test can give such important characteristics of the system as resonance frequency and Q-factor. By using these parameters the effective range of the vibration harvesting module can be estimated. Information concerning internal resistance and power output can be obtained only by testing, as it was demonstrated. Resonance frequency and effective operation range were obtained by two different tests and results of those tests were comparatively similar. It has been demonstrated that while Thevenin's equivalent can quite accurately describe power output characteristics this mathematical model fails to describe internal resonance due to its dependency on a current. Many other factors should be studied in order to properly describe both power output and internal resistance using the same model.

Acknowledgements

I would like to thank Ole-Erik Vestøl Endrerud and Tommy Svartvatn for supervision my thesis work and for the constructive and detailed feedback.

Besides my supervisors, I would like to thank Diana Starchenko for reviewing my thesis.

List of Figures

List of Tables

List of Acronyms

Contents

Chapter 1

Introduction

In the following chapter the general knowledge related to the energy supply problem for autonomous devices is provided, research questions are identified and brief overview of the literature used is presented.

1.1   Background

In the modern oil and gas industry there is a need in autonomous systems in order to submit important information about the current conditions in the well. Some devices use batteries, whereas others are powered by radio frequency waves.

For the certain applications, such as exploration wells, when there is no need to supply energy for a long period of time, batteries are the preferable choice. In some instances the system is required to operate during a long period of time and the batteries might need to be replaced. This is not necessarily possible in all applications, one of the examples being B-annulus pressure monitoring in a production well, where penetration of the wellhead is forbidden by the current regulations such as [1]. Moreover the issue becomes even more relevant given that batteries tend to degrade over time particularly in the high temperature environment [10].

If a device is being powered by radio frequency waves then special antennas should be installed inside and outside the pipe[3], which can lead to certain complications. At the same time these two antennas should be aligned as accurate as it is possible. In addition, transmitting radio signal through the metal is associated with considerable power losses.

Alternative solution to the issue of power supply to autonomous systems is to use energy harvesting modules. Since during drilling and production phases multiple sources of vibrations are present, these modules can be potentially used.

1.2   Problem definition

The objective of this thesis is to study the possibility to use harvesting modules for powering autonomous sensors.

The use of vibration harvesting modules for powering autonomous sensors in inaccessible locations such as B-annulus of the well can potentially decrease complexity of monitoring systems, significantly reduce installation time and costs. For the systems without external energy supply these modules can prolong lifetime of the equipment quite considerably, i.e. from several years up to life-time of the sensors. Therefore a need for the systems with external power supply can be eliminated since potentially enough energy can be harvested in well conditions. Some challenges

of using such devices in well conditions are being studied in this thesis. Research questions are formulated in the section 1.3.

1.3 Research questions

The following research questions are identified:

1. What is the response of the vibration harvesting module to the applied vibrations?

2. What is a proper mathematical model for describing behaviour of the vibration harvesting module?

3. What is the real power output of the device?

4. How wide is effective vibration spectrum of the vibration harvesting device?

1.4 Literature overview

In the process of writing this thesis it was essential to use literature covering not only energy harvesting in general, but also information related to electronics, mechanics and several other fields of science and engineering.

In order to identify the need for the harvesting modules in subsea well equipment technical reports and material from oil and gas conferences were studied, such as [15]. In this source the problem of supplying energy to the sensors placed in inaccessible locations in the well is mentioned. However, [15] addresses specifically exploration subsea wells which are not intended to be used for a period of times comparable to lifetime of the field, and therefore do not need to utilise any additional modules besides conventional batteries. The objective of supplying energy to the autonomous systems in the well is getting more complex when one is taking into consideration limitations of application of certain technologies which are stated in national standards such as [5] and [1].

Problem of annulus pressure monitoring is getting more significant in production wells as during SPE conference in Stavanger [3] one of the few industrial solutions was presented. The setup presented at the conference provides all the necessary energy supply and data exchange for the whole lifetime of the field, however non-efficient technology of transferring both data and energy via Radio Frequency (RF) through the metal pipe is used.

Datasheets of integrated circuit [8], transistor [9], vibration motors [11] and [12] and other electronics were studied to design the setup given in the experiment. Considerable attention was paid to [16] as it is the document which contains overall information about all the piezoelectric modules of Mide Technology Corporation. In addition some recommendations and features related to test procedure were taking into consideration.

Information about prospective technologies, like the one described in [18], was studied. However, possible application of prospective technologies in well conditions is not studied in available sources even though it might potentially be a more efficient method of delivering energy and information rather than the methods used in the mentioned industrial solutions [3].

History of the piezoelectric modules is well described in [6], [14], and [13]. [6] provides description of considerable variety of applications which includes not only energy harvesting application but more conventional utilisation such as sensors of different purposes, emitters and receivers of ultrasound for distance measurement and data transmission. Also properties description of many piezoelectric materials is provided. [13] is focused on materials and designs for transmission and receiving of ultrasound waves. In [14] information about one of the designs of micro-generators for converting mechanical energy into electrical energy is given.

Effects of high temperature conditions on batteries during long periods of time are described in [10]. This paper can potentially provide a basis for estimation of battery lifetime for harsh well environment.

[4] supplies all the needed data for developing experimental setup including not only electric characteristics, such as maximum source and sink currents for various pins, but also information about dialect of `C` programming language for Arduino IDE.

For the sake of proper electric design [7] was used. It provides all the necessary information for developing electric circuits for current setup, and mathematical modelling of linear and non-linear devices. This knowledge was vital for correct evaluation of results of the experiment. Furthermore, [17] was used to represent and legitimately process experimental data.

Chapter 2

Theory

Harvesting energy is the process of converting energy from the external sources into electricity, capturing this energy and making it possible to use for autonomous devices. Typically energy harvesters can only supply a very limited amount of power, the energy source is presented in the environment and can be utilised without any effects on the structure, main function of the system, etc. Whereas external source of energy is available and free, cost of the produced electricity is not important, since the main purpose of the system is to power autonomous device.

The problem of supplying energy to autonomous system is still relevant because there is no universal solution to it. Each particular application is different and should be addressed individually. In this thesis the problem of power supply to such a devices in the well is being studied.

Examples of usage of the energy harvesters nowadays are provided below in the table 2.1.

Table 2.1: Some examples of energy harvesting application

Example	Energy source
Oceanographic monitoring buoys	Motion of ocean waves
Handheld calculators	Light
Sensors in heating systems	Heat
Cooling modules	Heat
Microbial Fuel Cell	Chemical energy

2.1 Energy harvesting versus energy transfer

It is important to understand the difference between harvesting energy and transferring energy. In case of energy transfer there is an emitter which generates heat, ultrasound, RF, etc intentionally, and there is a receiver which converts energy back to electricity. In case of energy harvesting there is no emitter, i.e., no device which main purpose is to generate a certain field or motion to transfer energy to the receiver. E.g. in a well Electrical Submersible Pump (ESP) is pumping oil up to the XT and it creates vibrations during operation, which can be harvested into electricity. As in another example, when RF emitting antenna is located inside a pipe and receiving antenna is located outside, energy is being transferred, not harvested.

2.2 Sources of energy

There is a number of types of energy that can be converted into electricity but not all of them are applicable to well conditions. They are being discussed further. Common energy sources for harvesting are written below:

Light

Harvesting energy of the light is done by PhotoVoltaics method which is exploiting photovoltaic effect of semiconducting materials. The end result is Direct Current (DC) electricity with low potential (approximately $0.5\,\mathrm{V}$). It has been widely used in handheld devices such as calculators and watches, however it is not applicable to the well conditions due to lack of sun light below the ground.

Wind

Harvesting wind energy is accomplished by using so-called 'micro-turbines': a small sized wind turbine which has low power output.

Vibrations

Vibrations are being converted into electricity directly using piezo elements. Equipment which is being used during drilling and production is emitting vibrations, so there is no need for a special energy transmitter: energy wasted into vibrations is being harvested and utilised. Detailed description of the principle of operation of the vibration harvesting modules is written in the section 2.4.

RF Nowadays, source of the RF waves are everywhere: mobile phones, satellites, TV/Radio towers, therefore a number of industrial products is using this particular energy source for supplying electric energy for the autonomous sensors. Another factor which needs to be pointed out is the simplicity of the RF harvesting modules: the part converting RF to electricity is the antenna which is in the most simple case consists of a piece of metal wire with a proper length.

In the case of well equipment, since there is no RF sources, emitter and receiver of the RF waves are used, thus this cannot be considered as an energy harvesting, but rather energy transmitting. This method can supply totally sufficient amount of power but transferring energy via RF waves through the metal pipe can be problematic due to the face that metal pipe acts as a faraday cage blocking electric fields.

Heat

In the presence of temperature difference, i.e., temperature gradient, electricity can be generated directly using Thermoelectric effect, which is occurring in the presence of two different joined metals. Electric potential of the element depends on the gradient and relationship is not necessary linear. Low potential DC is generated.

Ultrasound

A new field of development is usage of the ultrasound to transmit energy. This method can be used in metal structures but because ultrasound wave dissipates fast, the usage of this technique can be limited. Also this method requires installation of the ultrasound transmitter and receiver[18]. It is very promising for constructions like a submarine.

2.3   Sources of vibrations in a well

As it stated below, there are multiple sources of the vibrations during drilling and production including:

- Vibration from drilling bit

- Cavitation during gas lift

- Vibrations from ESP (Electric Submersible Pump)

- Flow induced vibrations (e.g. from choke valve)

During the **drilling phase**, there is a number of powerful sources of vibrations, which are being emitted by drilling equipment including drilling bit and hydraulic systems of the rig.

During the **production phase** sources of vibrations are different depending on how oil or gas are being produced. For gas wells only flow induced vibrations can occur.

2.4   Principle of operation

Vibration harvesting modules exploit so-called 'piezoelectric effect'. It is an effect of accumulating electric charge in solid materials with specific properties as reaction to applied mechanical strain. The following effect was first observed and described by French physicists Jacques and Pierre Curie in 1880 [13]. Effect occurs only in a certain solid materials such as ceramics and crystals. Gautschi in [6] gives the following definition of the nature of the effect: "The piezoelectric effect is understood as the linear electromechanical interaction between the mechanical and the electrical state in crystalline materials with no inversion symmetry". Also, it is important to mention that the effect is reversible, meaning applying AC electricity to the crystal will cause mechanical oscillations (so-called 'reverse piezoelectric effect').

Piezoelectric effect in quartz is shown on the figure 2.1: during tension and compression of the crystal excessive charges are being formed.

Despite this effect being know for at least a century, harvesting vibrations has only been studied since the late 1990s [14]. Being under alternating mechanical strain (i.e., vibration), piezoelectric module produces AC electricity with magnitude up to hundred of volts. Since modern electric IC (Integrated Circuits) are using DC up to 5 V (in autonomous low-consumption
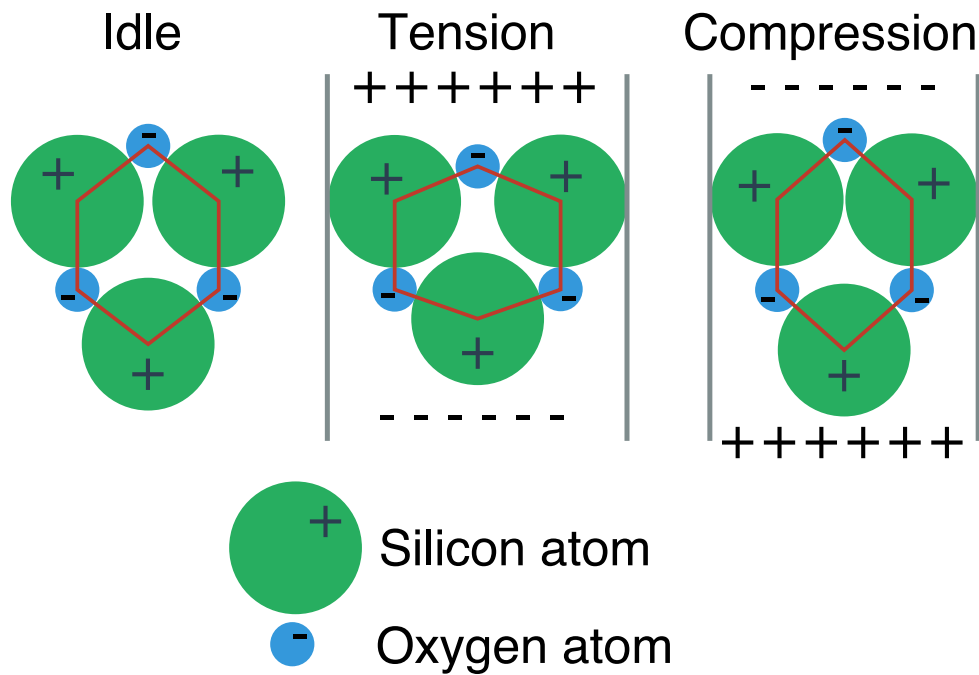
Figure 2.1: Illustration of piezoelectric effect in Silicon Oxide (Quartz)

devices up to $3\,\mathrm{V}$) as a power supply voltage, piezoelectric module cannot be used without special treatment. Typical piezoelectric module has power output in order of milliwatts, which can be enough for certain applications.

Piezoelectric module is shown on figure 2.2. It consists of the following parts:

Piezoelectric unit is a multi-layer composition which contains piezoelectric materials as well as isolation layers and electricity conducting layers.

Tip mass is an optional part of the device which tunes harvesting module to a specific frequency by decreasing its effective frequency operating range but significantly increasing response of the module.

Holding device is used to rigidly fix the harvesting module.

Electric contacts are providing electric output of the module. Internally they are connected to conducting layers inside the piezoelectric unit.

When vibrations are being applied to the harvesting module it starts to oscillate at the vibration frequency causing alternating strain of the piezoelectric materials which is generating electric potential difference at the output.

2.5   RMS

In order to make analysis of periodical sinusoidal waveforms easier so-called Root Mean Square (RMS) measure is used. Alternating Current (AC) electricity effect on purely resistive load is equal

Figure 2.2: Generic piezoelectric module

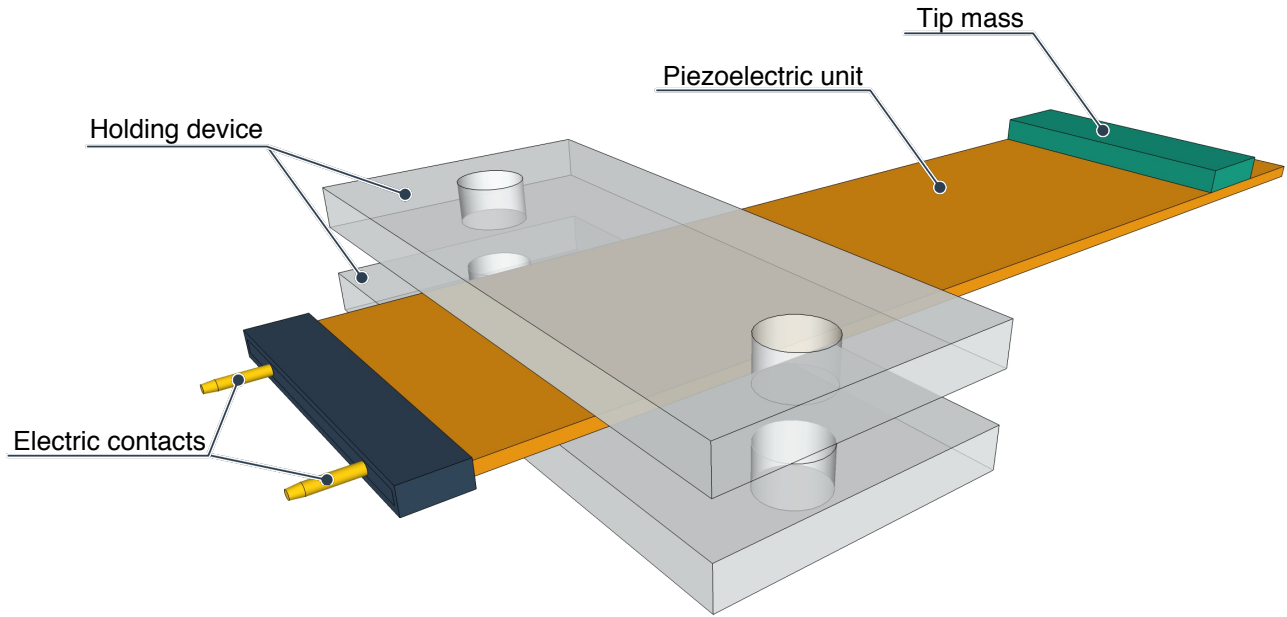to the effect of DC electricity with RMS magnitude on the same load [7]. For sinusoidal waveforms RMS units (voltage, current) are related to amplitudes as follows:

$$\text{RMS} = \frac{\text{Amplitude}}{\sqrt{2}} \tag{2.1}$$

2.6 PWM

For power control of the vibration motors so-called Pulse-Width Modulation (PWM) is used. PWM is a technique for manipulating the switch element and therefore load by letting it to be only in two states: on and off. This approach is very efficient because power loss on the switching element is low due to short transition periods (turning off and on) comparing to conducting periods (keeping on or off state). Usually switching power losses are much higher (dozen times or more) than conducting losses, which is why it is important to keep switching periods as short as possible. At the same time continuity of the operation of the device is provided by inertial effects, e.g., mass inertia in case of motors, i.e., load will operate in the same manner as being supplied with DC of lower magnitude. This state will naturally be obtained in condition when PWM frequency is high enough. Lower limit of the frequency depends on inertial properties. In most cases for electric motors inertia is high enough even at frequencies such as 10 kHz. However, it is recommended to use at least 20 kHz for PWM in order to prevent humans from being disturbed by generated sounds (human's ear cannot hear sound with frequency higher than 20 kHz).

General PWM waveform is shown on the figure 2.3. Only energy in hashed area is being supplied to the load. Transition timings are not shown.
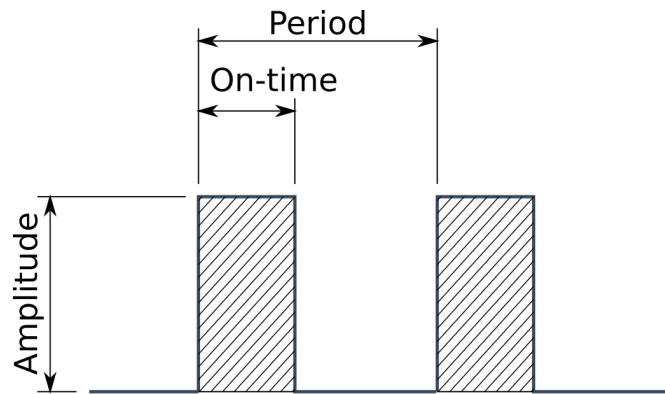
Figure 2.3: General PWM waveform

2.7 Thevenin's theorem
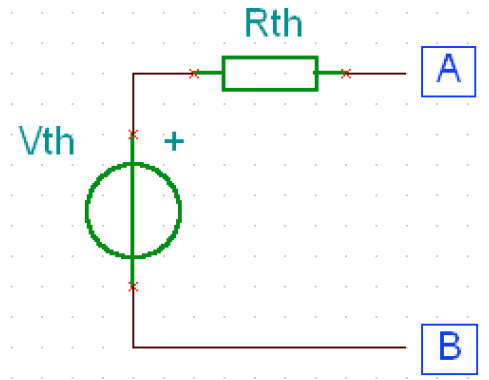
Figure 2.4: Thevenin's equivalent

Originally Thevenin's theorem was applied only to DC circuits, but by usage of impedances makes this theorem applicable also for AC circuits (impedance of resistance is equal to its resistance [7]). So-called thevenin's equivalent with A and B ports is shown on the figure 2.4. This theorem gives a way of representing circuit with linear elements by series combination of voltage source V_{th} and thevenin resistance R_{th}. Linear devices are devices which voltage-current characteristics can be expressed using linear relationships. Example of linear elements are: resistance, dependent and independent voltage and current sources.

This theorem can be used to represent any type of electricity source devices such as batteries or, in this case, piezoelectric modules. It can be achieved due to linearity of characteristics on wide interval of operation. In case of non-linearity internal resistance can be described as a function of known variables, not just a constant.

2.8 Maximum power transfer theorem

Power transfer process can be describe by 2 parameters: efficiency and power transfer ratio. Efficiency by definition is equal to the ratio of power transferred to the load to power generated by power source. For Thevenin's equivalent, power transferred to the load is calculated as shown

in equation (2.2).

$$P_L = I^2 \times R_L \tag{2.2}$$

Power generated by the power source can be found as described in equation (2.3).

$$P_V = I \times V \tag{2.3}$$

Therefore, efficiency coefficient is equal to expression shown in equation (2.4).

$$\eta = \frac{P_L}{P_V} = \frac{I^2 \times R_L}{I \times V} = \frac{I \times R_L}{V} \tag{2.4}$$

Current in the circuit is equal to the following equation:

$$I = \frac{V}{R_L + R_{\text{th}}} \tag{2.5}$$

By substitution equation (2.5) into equation (2.4) the following equation is being obtained:

$$\eta = \frac{I \times R_L}{V} = \frac{V}{R_L + R_{\text{th}}} \times \frac{R_L}{V} = \frac{R_L}{R_L + R_{\text{th}}} \tag{2.6}$$

Equation (2.6) shows that the higher R_L the higher is η, and reaching 1.0 when $R_L \to \infty$.

By substituting equation (2.5) into equation (2.2) the following equation is derived:

$$P_L = \frac{V^2}{(R_L + R_{\text{th}})^2} \times R_L \tag{2.7}$$

Maximum of the P_L function equation (2.7) is achieved when derivative by R_L is equal to zero.

$$\frac{\mathrm{d}}{\mathrm{d}R_L} P_L = \frac{V^2}{(R_L + R_{\text{th}})^2} + \frac{V^2 R_L(-2)}{(R_{\text{th}} + R_L)^3} = \frac{V^2}{(R_L + R_{\text{th}})^2}\left(1 - 2\frac{R_L}{R_{\text{th}} + R_L}\right) \tag{2.8}$$

$$0 = \frac{V^2}{(R_L + R_{\text{th}})^2}\left(1 - \frac{2R_L}{R_{\text{th}} + R_L}\right) \tag{2.9}$$

$$1 = \frac{2R_L}{R_{\text{th}} + R_L} \tag{2.10}$$

$$2R_L = R_L + R_{\text{th}} \tag{2.11}$$

$$R_L = R_{\text{th}} \tag{2.12}$$

Equation (2.12) shows that the maximum power transfer is achieved when resistance of the load R_L is equal to the internal resistance of the power source R_{th}.

2.9   Damped oscillations

Damped oscillations are oscillations which decaying over time. They can be classified into 3 categories: under damped, critically damped and over damped oscillations. Under damped oscillations are decaying slowly: more than 2 cycles; critically damped oscillations are decaying fast: 1 or 2 cycles; and over damped oscillations are not involving any periodic oscillations.

Damping coefficient ζ is used to classify the oscillations. It can be found as follows:

$$\zeta = \frac{\alpha}{\omega_0} \tag{2.13}$$

where:

α = is the decay ratio $[\text{s}^{-1}]$

ω_0 = is the natural angular frequency of the oscillations $[\text{s}^{-1}]$

Decay ratio α is exponential decay in form of $\exp(-\alpha t)$. General form of under damped oscillations is shown below [2].

$$v = ae^{-\alpha t}\sin(\omega t + \phi) \tag{2.14}$$

Factor, which shows ratio of energy stored in the system to energy lost per cycle, is called Q-factor and can be found as follows [2]:

$$Q = \frac{1}{2\zeta} \tag{2.15}$$

Chapter 3

Methodology

In order to answer the research questions identified in section 1.3 a test of the Vibration Harvesting Module (VHM) should be performed. In the following sections of this chapter design procedure is described in details.

3.1 Methods and materials

List of the equipment used in the following experiment is presented below:

Extech MN35 True-RMS multimeter

Tektronix MSO2104 Bench-top 5 channel oscilloscope

Tenma 72-10505 programmable power supply

Test installation is described further.

BPS BB400 84 mm by 54.3 mm breadboard

Diagram of the structure of the installation is shown on the figure 3.1. Vibrations are being emitted by Vibration Emitting Module (VEM), transmitted via Vibration Medium (VMe) to the VHM, where they are being converted into electricity and measured.

Parts used in the test installation are listed in table 3.1 with brief description. Specific description is written in separate sections for each module: 3.2 for VEM, 3.3 for VHM.

Electric parts of VEM and VHM can be assembled on Printed Circuit Board (PCB) or breadboard. For the sake of simplicity and convenience breadboard is used for this experiment. It is acceptable because non of the parts are operating at high frequencies, voltages or currents. Also breadboard provides much more flexibility which is vital for experiments.

Vibration Motors (VMo) and Piezoelectric Unit (PU) are fixed on the VMe which provides mechanical link between two elements. In the experiment simple steel plate is used. Damping material under the VMe is used to fix the whole installation to the table.

3.2 Vibration Emitting Module (VEM)

According to the figure 3.1 VEM consists of the following parts:
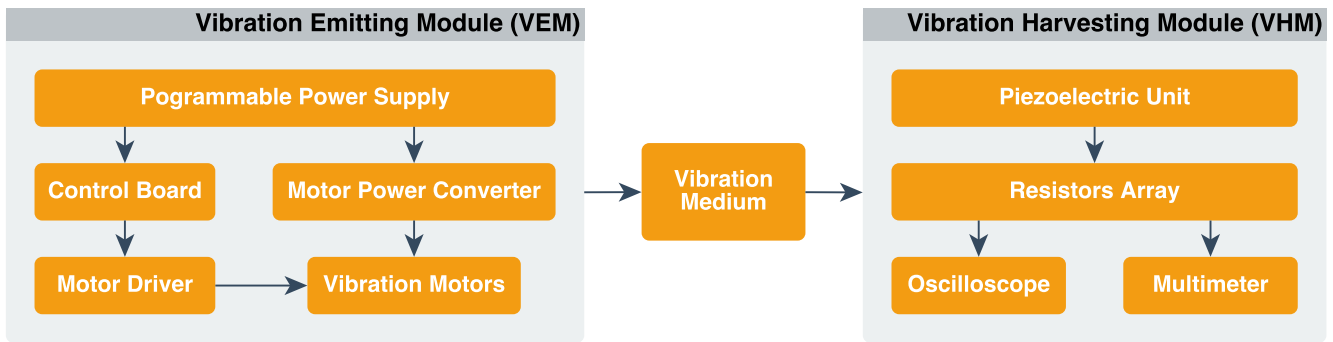
- VMo

Figure 3.1: Structure of the installation

- Control Board

- Motor Driver

- Motor Power Converter

Each part of the VEM is described in the following subsections.

3.2.1 VMo

Two VMo **28821** and **28822** by **Parallax** were chosen for emitting vibrations. The reason for using two motors is to test response of the harvesting module to different sources of vibration. Flyback diode `D1` is used to protect MOSFET `Q1` from voltages spikes due to inductivity of the motors `M1` and `M2`.

3.2.2 Control Board

VMo are being controlled by **Arduino UNO** development board, which can provide an easy way of regulating the motors and therefore mode of their vibration. This device has been chosen due to following reasons:

Easy to develop firmware

Arduino devices are extremely easy to program from both software and hardware points of view. Firmware for the Arduino devices is written in the open-source native Integrated Development Environment (IDE) which is available for Windows, Linux, and Mac OS X operation systems. Dialect of `C` programming language can be studied in a short time based on high number of tutorials and examples provided by the community. Arduino can be easily connected to a PC or Mac using general USB-B cable without the need to install additional software (drivers are standard). Flashing process is done in the IDE without any need for addition software.

Table 3.1: Modules parts

VEM				
Label	Manufacture	Model	Qty	Description
M1	Parallax	28821	1	Vibration motor 3 V 90 mA 9 000 RPM
M2	Parallax	28822	1	Vibration motor 3 V 250 mA 12 000 RPM
B1	Arduino	UNO Rev.3	1	Single-board microcontroller
U1	TI	LM317	1	3-terminal linear voltage regulator
Q1	Vishay	IRL620	1	N-Channel Power MOSFET 200 V 5.2 A
C1	TDK	0.1 µF	1	Multilayer Ceramic Capacitors 50 V 5%
C2	TDK	1 µF	1	Multilayer Ceramic Capacitors 50 V 5%
R1	Vishay	1 kΩ	1	Metal Film Resistors 1/4 W 1%
R2	Vishay	330 Ω	1	Metal Film Resistors 1/4 W 1%
R3	Vishay	240 Ω	1	Metal Film Resistors 1/4 W 1%
R4	Vishay	33 Ω	1	Metal Film Resistors 1/4 W 1%
D1	Fairchild	EGP10B	1	1 A fast diode
VHM				
Label	Manufacture	Model	Qty	Description
X1	Mide	PPA-1001	1	Piezoelectric Unit
RP	Bourns	4116R-1-472LF	2	4.7 kΩ RA

Easy to control

It is very simple to control execution of the firmware using any hyper terminal tool provided with operation system or installed separately (one is included into IDE).

For a proper operation motors should be supplied with 3.0 V DC with current up to 120 mA [11] and 680 mA [12] respectively, which is above the Arduino UNO board maximum current pin output (which is 50 mA for 3.3 V Pin) [4]. Therefore, a special driver should be used to control the motors.

To control the vibration mode of VMo PWM is used. Standard Arduino's method `analogWrite` is utilised for creating PWM signal.

Source code of the firmware for Arduino UNO is provided below:

```
void setup() {
  // start serial port at 9600 bps and wait for port to open:
  Serial.begin(9600);
  while (!Serial) {
    ; // wait for serial port to connect.
    // Needed for native USB port only
  }

  pinMode(6, OUTPUT);    // PIN6 for PWM output
}

void loop() {    // main loop of the program

  // execute when receiving data via serial port
  if (Serial.available() > 0) {

    // parse serial port buffer to integer value
    int inVal = Serial.parseInt();

    // stop reading after receiving end of the line
    if (Serial.read() == '\n') {
      Serial.print("new duty cycle value received: ");

      // mapping from 0-100 range to 0-255 range
      int newVal = map(inVal, 0, 100, 0, 255);

      Serial.print(inVal);        // show received value
      Serial.print(" ");
      Serial.println(newVal);    // show mapped value

      analogWrite(6, newVal);    // set new duty cycle on PIN6
    }
  }
}
```

3.2.3 Motor Driver

MOSFET **IRL620** by **Vishay Intertechnology** has been chosen due to ability to be driven by 5 V Pin output of the Board without any special controlling circuits. It is an N-channel "Logical" MOSFET with maximum voltage up to 200 V and current up to 5.2 A [9], which is more than sufficient for the application. It is connected to the `PIN6` of the Board through current limiting resistor `R4` to prevent so-called "ringing" which can be caused by parasitic inductance of the wire and input capacitance of the MOSFET forming a `RLC` circuit. Impulse response of the `RLC` circuit is damped oscillation with amplitude depending on the damping properties and frequency nearly equal to resonant frequency of the `RLC` circuit. This application does not require high switching frequency thus it is more suitable to avoid the effect of "ringing" at all by making turning-on of the MOSFET slow enough by limiting the charging current.

Maximum gate current I_g for `IRL620` is:

$$I_g = \frac{V_{cc}}{R_4} = \frac{5\,\text{V}}{33\,\Omega} = 0.152\,\text{A} \tag{3.1}$$

where:

$V_{cc} = 5\,\text{V}$ is the output voltage of the Arduino `PIN6`

Estimated switching-on time of the `IRL620` is:

$$t = \frac{Q_g}{I_g} = \frac{16\,\text{nC}}{152\,\text{mA}} = 105\,\text{ns} \tag{3.2}$$

where:

$Q_g = 16\,\text{nC}$ is the total gate charge of the `IRL620`

3.2.4 Motor Power Converter

Arduino UNO board is not able to supply enough current for the operation of the motors, so power converter from potential of 5 V down to 3 V should be used. Module on basis of linear voltage regulator **LM317** by **Texas Instruments** is chosen as an easy and sufficient solution in terms of stability, size, power output and efficiency. It can supply up to 1.5 A current [8] which is sufficient for providing electric energy for VMo. According to [8] only 2 external resistors are required for 3 V output. Output voltage does not depend on the input voltage as long as input voltage is higher than desired output for the saturation voltage.

The resistors `R2` and `R3` are setting up the output voltage of the regulator `LM317`. Formula

for the output voltage is provided in the [8]:

$$V_{out} = 1.25\,\text{V} \times \left(1 + \frac{R_2}{R_3}\right) + I_{adj} \times R_2 \tag{3.3}$$

where:

$I_{adj} = 100\,\mu\text{A}$ current from adjustment terminal. This term can be neglected due to insignificant influence to the result.

By plugging in values for the R2 and R3 into equation (3.3) the output voltage is:

$$V_{out} = 1.25\,\text{V} \times \left(1 + \frac{330\,\Omega}{240\,\Omega}\right) = 2.97\,\text{V} \tag{3.4}$$

which is in the operating range of the VMo.

Capacitors C1 and C2 are needed for smoothing input and output voltages, their recommended capacitance values are specified in the [8].

Maximum power dissipation of the LM317 is calculated as follows:

$$P = (V_{in} - V_{out}) \times I_{max} = (5\,\text{V} - 3\,\text{V}) \times 1\,\text{A} = 2\,\text{W} \tag{3.5}$$

where:

$V_{in}\quad = 5\,\text{V}\quad$ is the input voltage

$V_{out}\quad = 3\,\text{V}\quad$ is the output voltage

$I_{max}\quad = 1\,\text{A}\quad$ is the maximum current

1 A is an exaggerated value, it is used to make upper approximation of the dissipated power. 2 W will cause temperature of the junction rise up to:

$$T_{junction} = T_{ambient} + P \times R_{\theta JA} = 20\,°\text{C} + 2\,\text{W} \times 23.3\,°\text{C/W} = 66.6\,°\text{C} \tag{3.6}$$

where:

$T_{ambient} = 20\,°\text{C}\qquad$ is the ambient temperature

$R_{\theta JA}\quad = 23.3\,°\text{C/W}\quad$ is the junction-to-ambient thermal resistance [8]

Obtained result is in the operation range of the LM317 Integrated Circuit (IC).

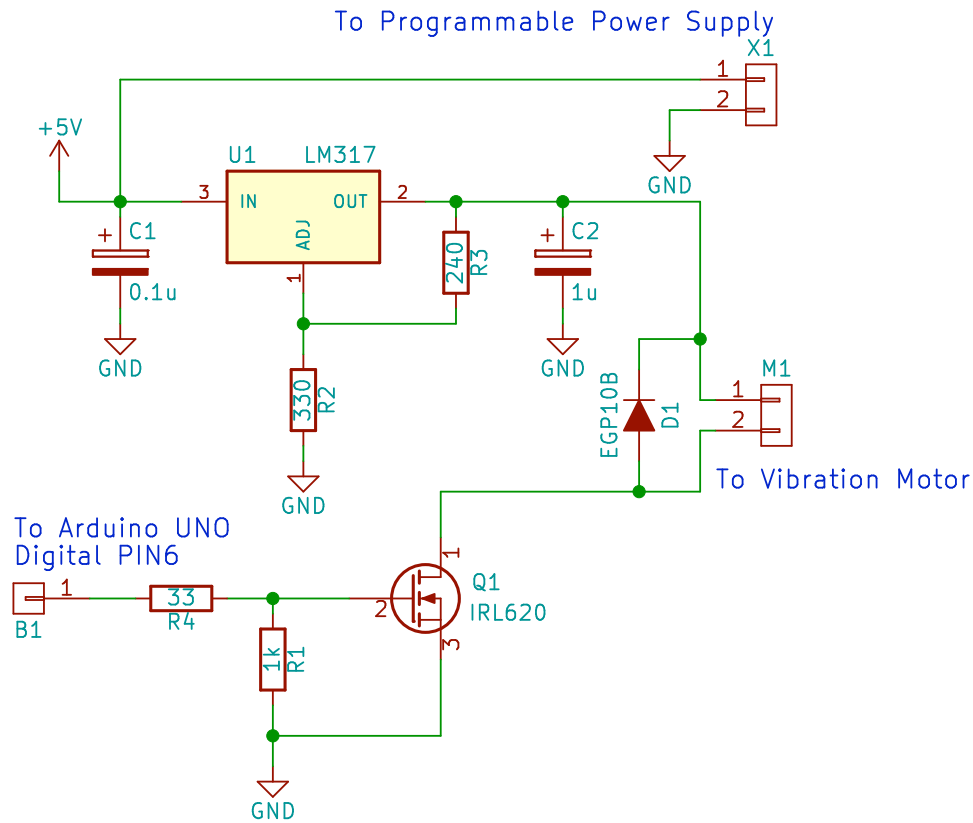Electric circuit of the VEM is shown on the figure 3.2.

Figure 3.2: VEM electric circuit

3.3 Vibration Harvesting Module (VHM)

As shown on the figure 3.1, VHM includes the following parts:

Piezoelectric Unit (PU)

PU is the harvesting unit. **PPA-1001** by **Mide Technology** was chosen due claims of the Mide this module being the most cost effective option [16]. It can provide up to $4.4\,$mW in resonance. Maximum possible output voltage is stated to be $120\,$V in both polarities, but according to provided table in the [16] maximum expected voltage can be up to $17.3\,$V.

Resistors Array (RA)

In order to measure response of the PU on different loads RA is used. It consists of 2 x **Bourns 4116R-1-472LF** each being an array of 8 x $4.7\,$kΩ resistors. In the circuit they are connected in series, providing maximum resistance up to $(8 \times 2) \times 4.7\,\text{k}\Omega = 75.2\,\text{k}\Omega$.

Oscilloscope

Tektronix MDO3024 oscilloscope is used due to availability in the lab. Main purpose of the oscilloscope in this experiment is to register the response (waveform) of the PU to the vibrations. Measurements of RMS voltage is done by True-RMS multimeter. Registered response is logged and studied.

Multimeter

Any True-RMS Multimeter is suitable for this application. **Extech MN35** is used due to availability. Multimeter and Oscilloscope are both used as measuring tools for purpose of checking reliability of the data.

Electric circuit of the VHM shown on the figure 3.3. RA is used to select different load for the PU by connecting ground wire from `X1` to different pins of `PR1` and `PR2`. On the figure 3.3 `X1` is connected to the 8th pin of the `PR2` providing maximum available load of $75.2\,\text{k}\Omega$.
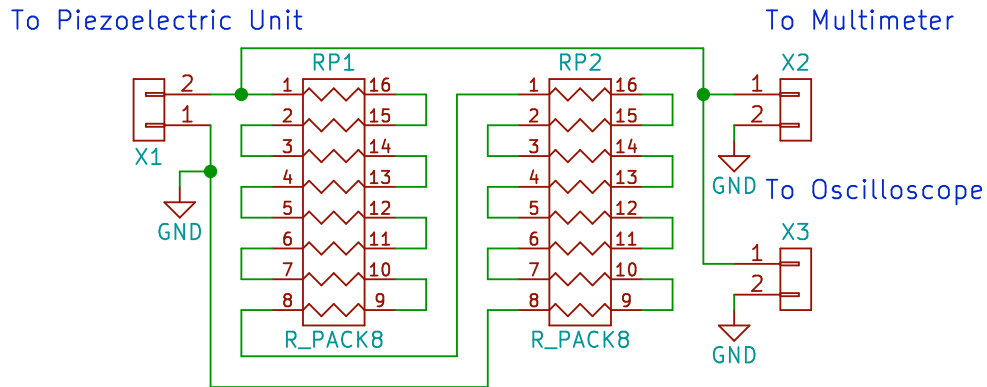
Figure 3.3: VHM electric circuit

3.4 Overview of the testing setup

Assembled electric components of both VHM and VEM modules are shown on the figure 3.4. On the right part of the assembly factory manufactured Arduino UNO is installed. On the left side breadboard with mounted components is attached. Almost all the available breadboard space is used for the setup.
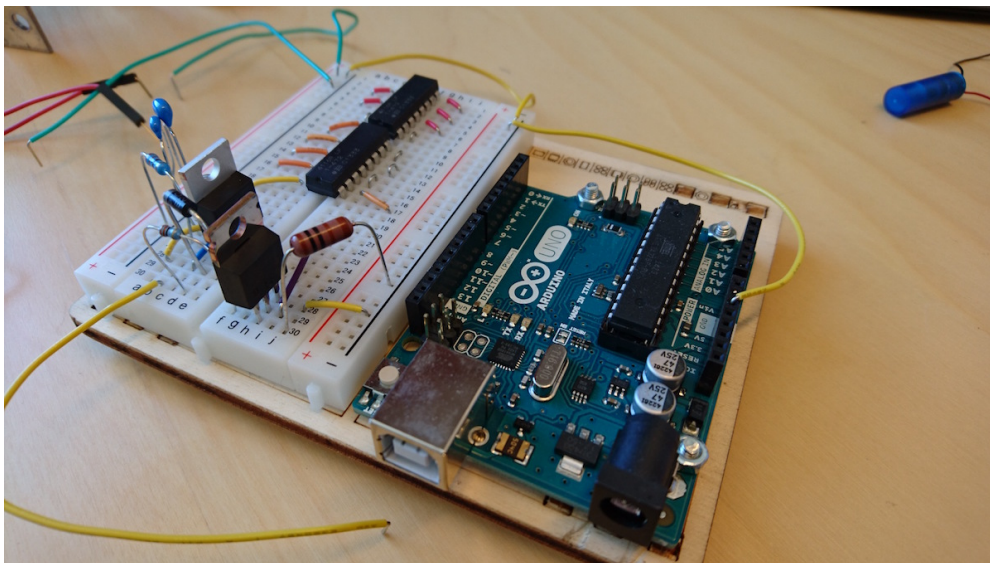

Figure 3.4: VHM and VEM assembly

Piezoelectric module with vibration motors are shown on the figure 3.5. They are mounted on the frame shown on the figure 3.6, which is used to fix mechanical components and to conduct vibrations, i.e. act as vibration medium specified on the figure 3.1.
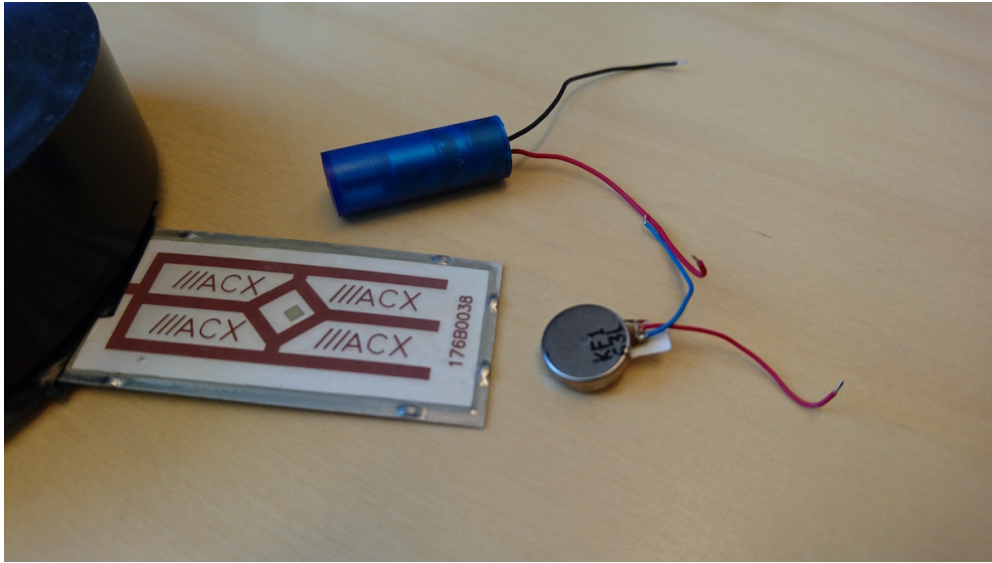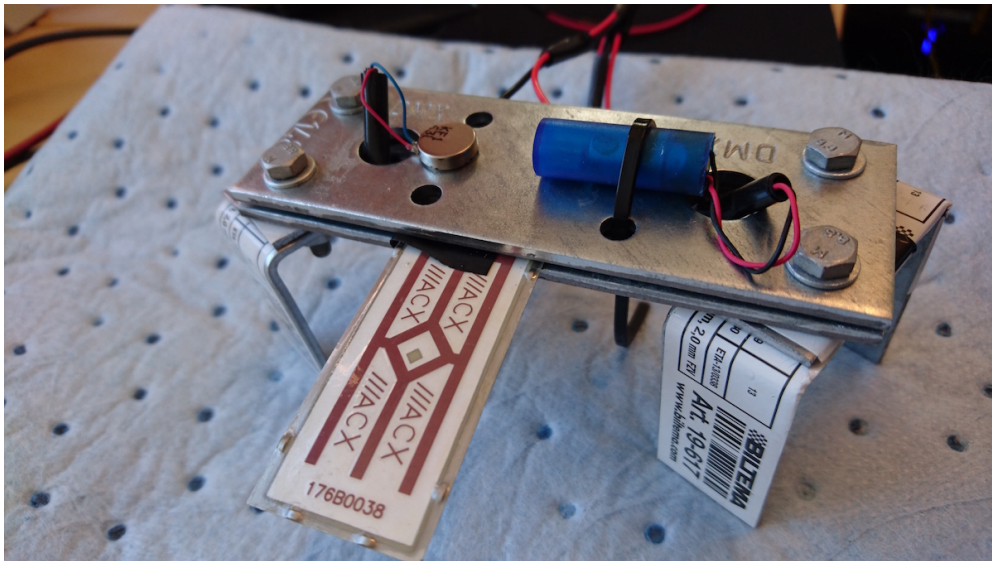

Figure 3.5: Piezoelectric module and vibration motors

Figure 3.6: Mounting frame

3.5   Experimental procedure

In this section procedure of conducting the experiment is given:

Assembling electric parts of VHM and VEM on the breadboard

In this step all the electric components of VHM and VEM should be 'plugged' into the holes in the breadboard as demonstrated on the figure 3.3 and figure 3.2. To accomplish this all the components should be in through-hole type of casing or, if some of Surface-Mount

Device (SMD) is used, wires should be soldered to the pins from one side and plugged into the breadboard from the other side.

Mounting VMo and PU to the VMe

VMo are attached to the VMe (steel plate) using adhesive materials. Piezoelectric Module is mounted inside the frame.

Connecting VMo to VEM and PU to VHM electronics

Wires from VMo should be connected to VEM and wires from PU to VHM according to the figure 3.2. Assembled breadboard is shown in the figure 3.7.
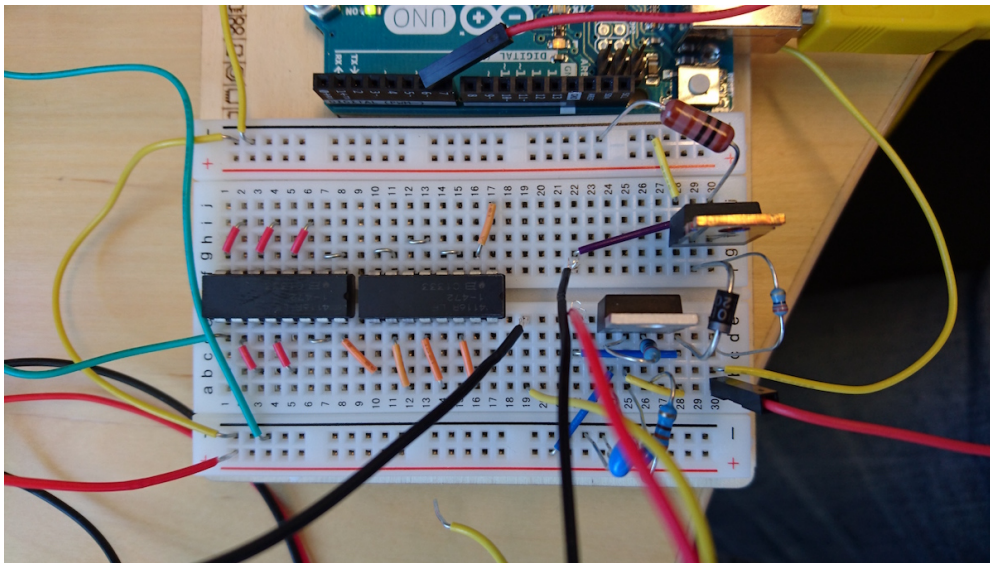

Figure 3.7: Assembled breadboard

Turning on VEM and getting readings from VHM for each specified mode of operation

VEM is being turned on desired settings which provides operation in range near the resonance. Oscillograms from Oscilloscope are being saved for each case. Duty cycle is being controlled by Arduino board through `RS-232` protocol from a PC station.

Performing natural oscillations test

Natural oscillations test is done by displacing the tip of the piezoelectric module and releasing it. Output waveform is being captured.

Calculation of current in the circuit and power output for each case

Current and power provided by VHM is calculated after receiving data. It is done using Ohm's law and definition of the electric power.

Ohm's law:

$$I = U/R \tag{3.7}$$

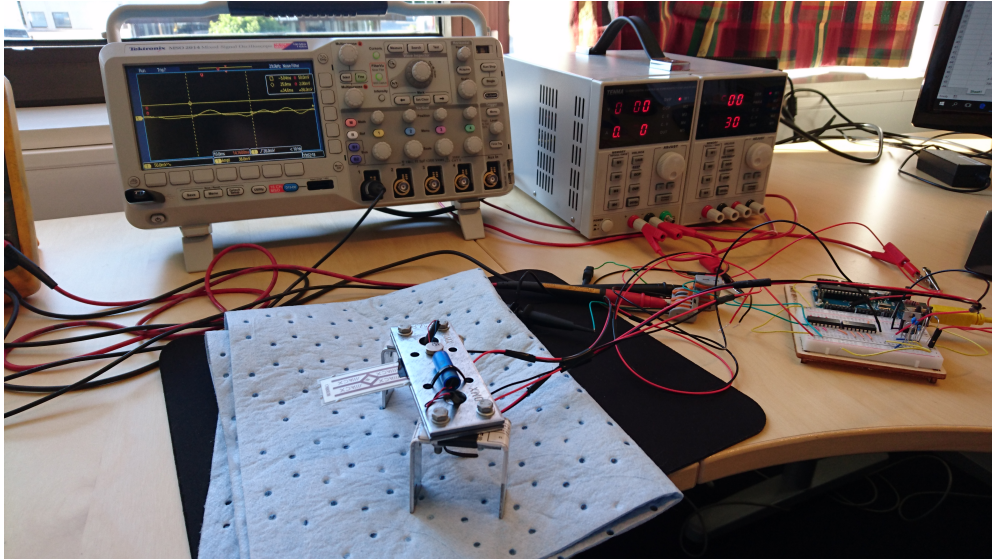Electric power:

$$P = U \times I = U^2/R \tag{3.8}$$

Figure 3.8: Test setup

Chapter 4

Results

Three types of experiments were performed: two experiments with induced vibrations by using two different vibration motors and one experiment with natural oscillations. Duty cycles specified in table 4.1 and in table 4.2 for the first and for the second tests respectively were used due to their ability to provided frequency range which is near the resonance frequency and twice the resonance frequency.

4.1 First vibration motor experiment

Results of the first vibration motor experiment are shown in table 4.1. Waveforms were quite stable, but it was not possible to achieve frequencies lower than 61 Hz. Waveforms of the open-circuit measurements are located in appendix section and figure's numbers are specified in table 4.1 as well.

4.2 Second vibration motor experiment

Results of the second vibration motor experiment are shown in table 4.2. This motor is much more powerful, but it has induced a lot of noises. Waveforms were not stable. Waveforms of the open-circuit measurements are located in appendix section and figure's numbers are specified in table 4.2 as well.

4.3 Natural oscillations tests

Natural oscillations test was performed three times with opposite directions of displacement and different displacements values. Waveforms are show in figure 4.1, figure 4.2, figure 4.3.

Table 4.1: 1st vibration motor test

Duty cycle, %	16	17	18	19	20	22	25	30	47
f, Hz	–	61	65	70	75	81	88	120	140
#	R_L, kΩ				Signal RMS, mV				
1	4,7		56	31	19,2	16,8	20,0	13,2		28,0
2	9,4		100	54,4	35,2	31,2	32,0	23,2	12,0	46,4
3	14,1		146	78	51,2	43,2	44,0	32,8		56,0
4	18,8		176	93,6	59,2	50,0	51,2	38,0	17,0	64,8
5	23,5		204	110	70,4	61,6	57,6	42,0		67,2
6	28,2		220	118	73,6	61,0	60,8	44,4	19,0	70,4
7	32,9	Motor is not working	240	128	80,0	69,6	64,8	47,6		70,4
8	37,6		248	131	82,4	67,2	66,4	47,6	20,0	72,8
9	42,3		260	140	88,0	75,2	67,2	50,0		68,8
10	47,0		268	140	86,4	72,0	68,8	50,0	21,0	72,0
11	51,7		272	148	92,8	76,8	68,8	51,6		70,0
12	56,4		280	148	90,0	73,6	70,4	51,0	21,6	75,2
13	61,1		288	152	93,0	78,4	69,6	52,8		70,0
14	65,8		288	152	95,0	75,2	70,0	52,0	21,6	73,0
15	70,5		294	154	97,0	78,4	70,4	53,6		70,0
16	75,2		296	154	97,0	76,0	71,2	52,0	21,6	76,0
17	∞		316	168	102,0	80,0	76,0	52,4	22,0	79,0
	Figure		B.1	B.2	B.3	B.4	B.5	B.6	B.7	B.8

Table 4.2: 2nd vibration motor test

Duty cycle, %		4	5	6	7	8	9	80
f, Hz		52	61	72	78	83	87	122
#	R_L, kΩ	Signal RMS, mV						
1	4,7	18	64	24	18	14	14	
2	9,4	42	136	44	34	28	26	
3	14,1	56	192	64	50	38	38	
4	18,8	80	224	76	66	44	46	
5	23,5	84	264	94	64	56	52	
6	28,2	100	288	96	74	60	56	
7	32,9	100	320	106	74	60	62	
8	37,6	116	328	104	82	64	60	Too much noise
9	42,3	110	360	114	84	65	62	
10	47	130	352	114	84	68	62	
11	51,7	116	360	116	84	68	62	
12	56,4	130	376	118	84	68	62	
13	61,1	120	376	124	84	70	64	
14	65,8	130	376	124	84	68	62	
15	70,5	136	384	124	86	70	62	
16	75,2	134	408	124	90	70	62	
17	∞	142	408	130	88	72	62	90
Figure		B.9	B.10	B.11	B.12	B.13	B.14	B.15
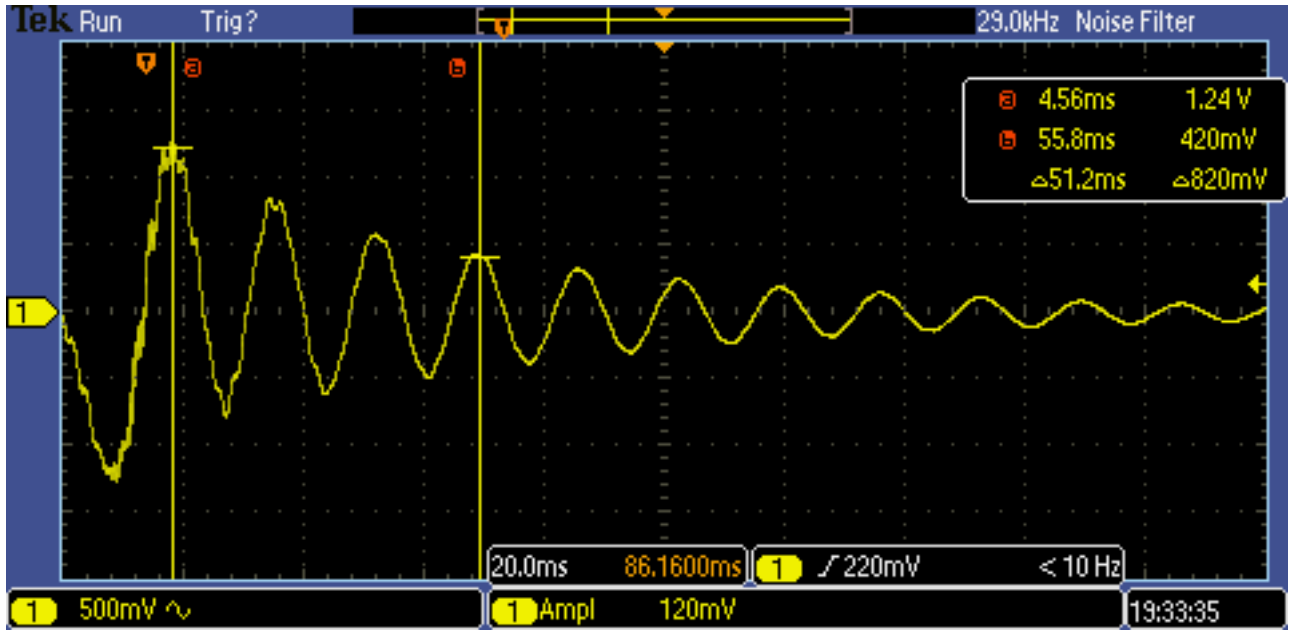
Figure 4.1: Natural oscillations test #1
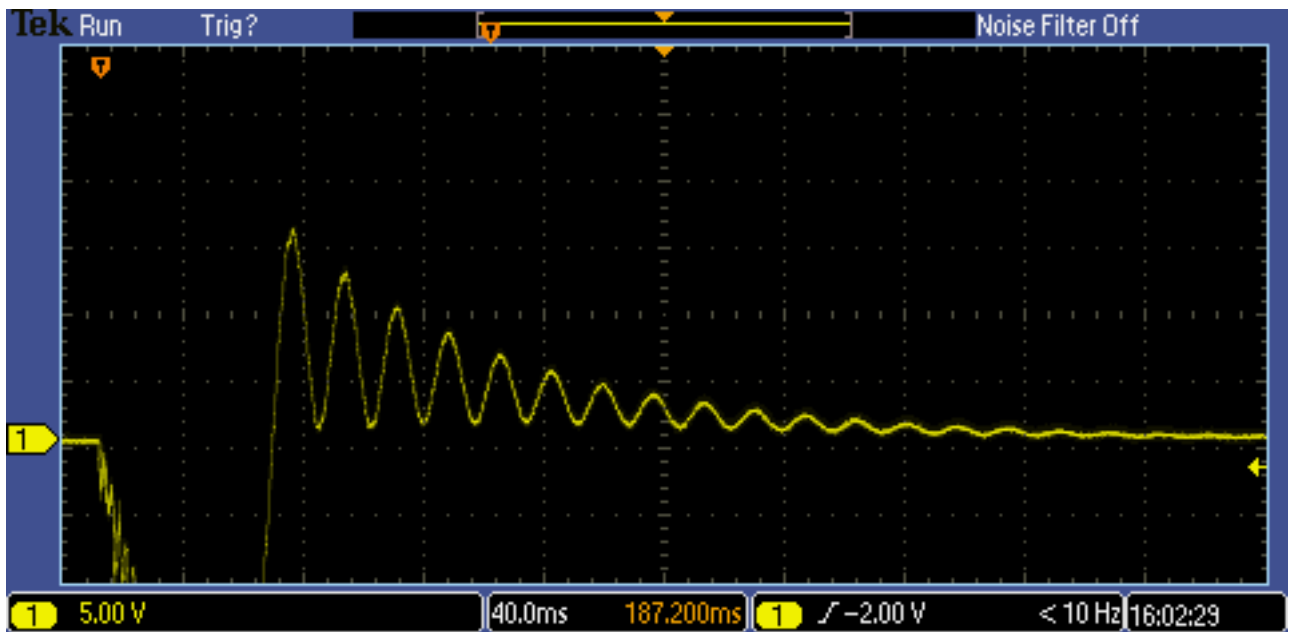
Figure 4.2: Natural oscillations test #2
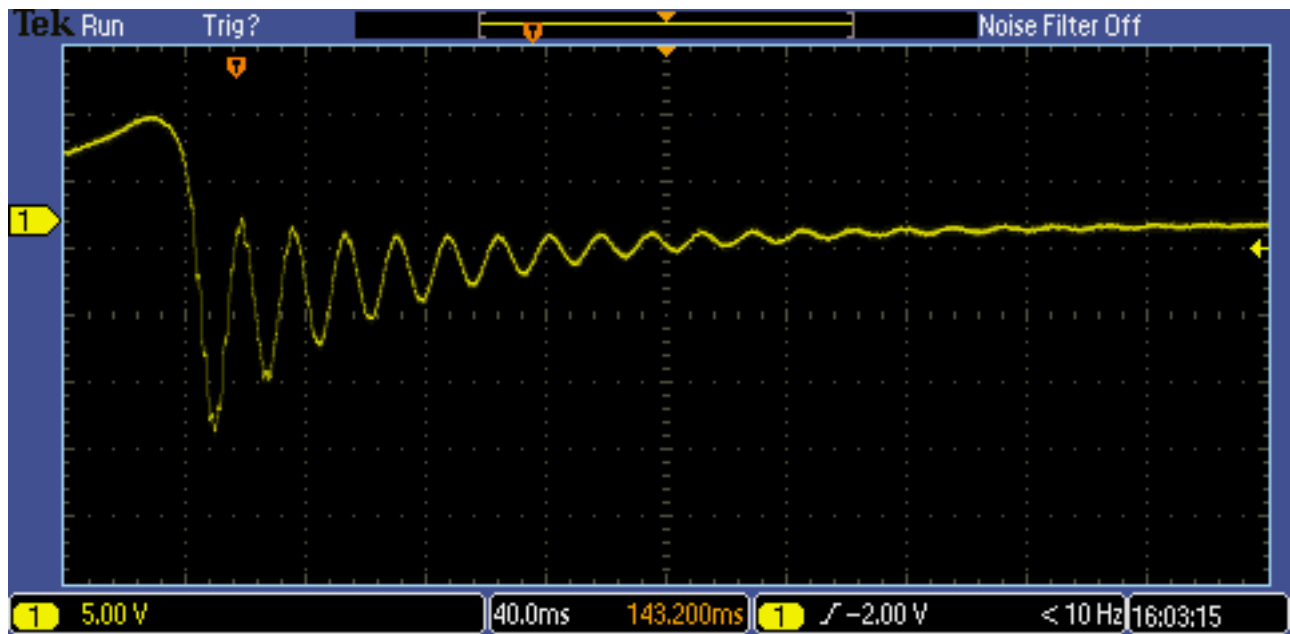
Figure 4.3: Natural oscillations test #3

Chapter 5

Discussion

5.1 Response of the VHM

As seen from the logged waveforms, the response of the VHM is AC with frequency equal to a vibration frequency. Amplitude of the response depends on the frequency of vibration as well as on the load resistance. According to the data obtained by the experiment, the response is maximum at the frequency of approximately $61\,\mathrm{Hz}$.

Because the response is a regular sinusoidal waveform we can simplify all the calculations by using RMS values instead of functions of *sin* or *cos* functions. The basis of this approximation is described in details in the section 2.5. Therefore the conclusion is made that it is possible to treat AC as DC.

5.2 Converting AC response to RMS equivalent

For a regular sinusoidal wave as described in the section 2.5 RMS equivalent value is given as:

$$V_{RMS} = \frac{V_a}{\sqrt{2}} \tag{5.1}$$

$$I_{RMS} = \frac{I_a}{\sqrt{2}} \tag{5.2}$$

where:

V_a = is the voltage amplitude

I_a = is the current amplitude

By applying equation (5.1) and equation (5.2) to the results of the experiment we get the following:

5.3 Electric model of the VHM

It is visible from the result that there is a non-linear response of the VHM, not only according to resistance of the load but also to frequency of the vibrations, namely there are obvious resonance points at which power output is much higher. In addition resonance points were observed at a frequency approximately twice higher than natural frequency.
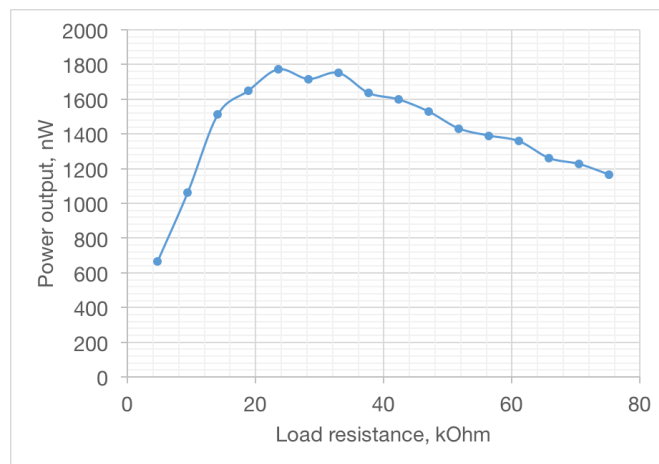
In order to choose a proper mathematical model voltage figure 5.1a, current figure 5.1b and power outputs figure 5.1c are shown below. Mathematical model is selected by comparing figures

to theoretical ones starting from the most basics ones.
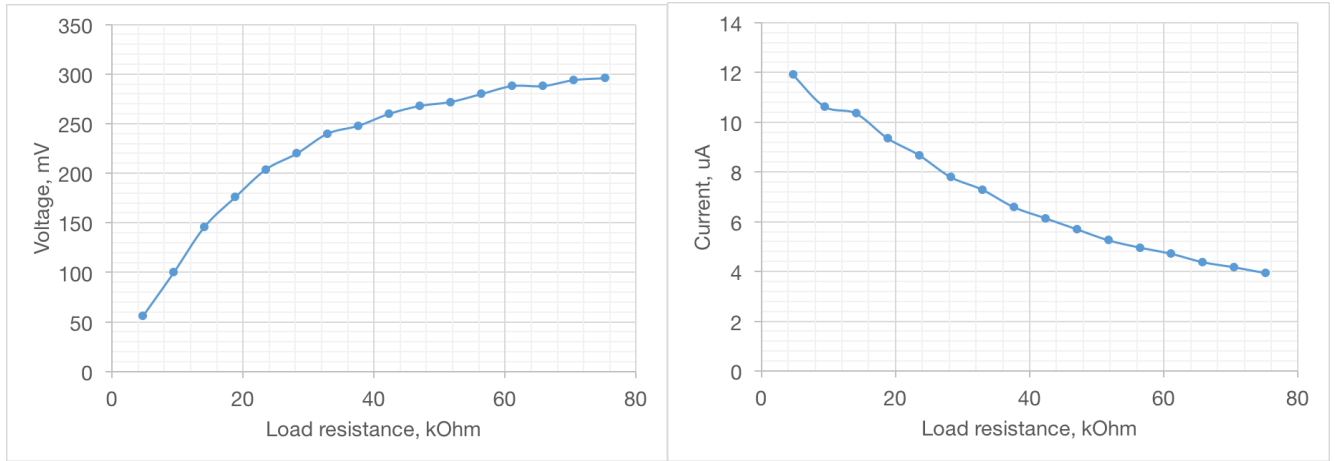
(a) Voltage output

(b) Current

(c) Power output

Figure 5.1: Parameters of the system at frequency close to resonance

### 5.3.1 Electric models overview

Voltage source

One of the most simple mathematical models to consider is a voltage source model. Voltage source is an ideal component which is supplying constant voltage independently on load connected to it [7]. Equivalent circuit is shown on the figure 5.2a. Assumed parameters are shown in table 5.1.

Table 5.1: Voltage source example parameters

Parameter	Value
VS1, V	10
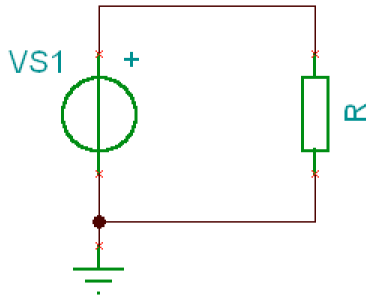
(a) Voltage source model circuit
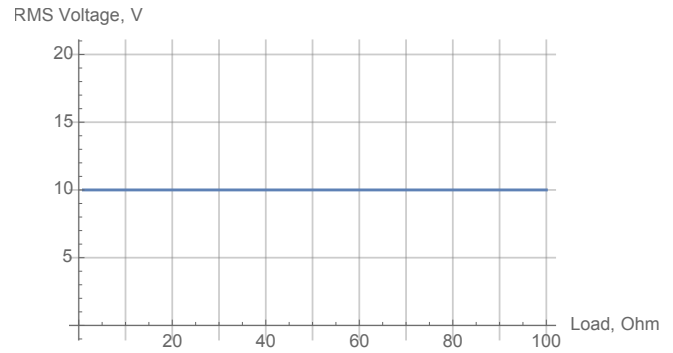
(b) Voltage output
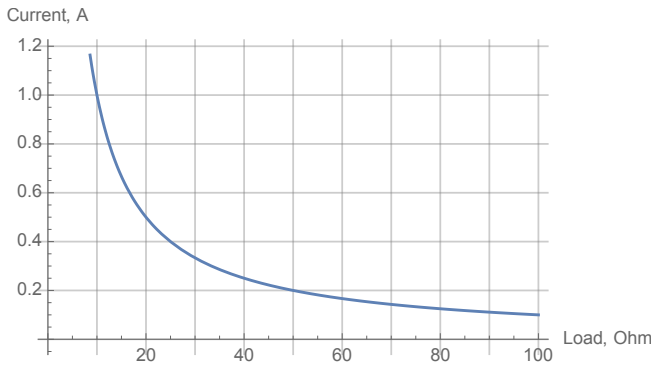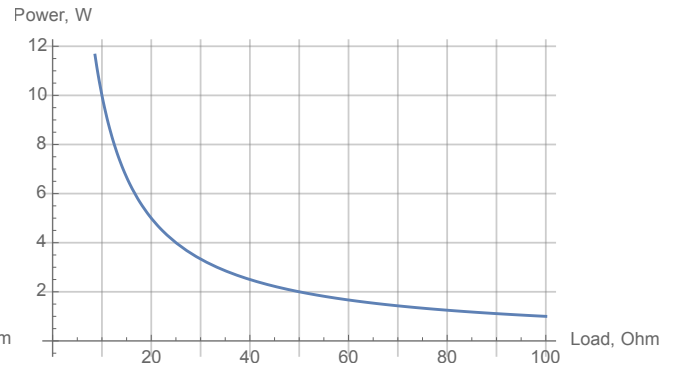
(c) Current output

(d) Power output

Figure 5.2: Voltage source model figures

The curve for voltage versus load presented on the figure 5.2b. figure 5.2c shows relationship current output of the circuit as a function of load. Power output curve for the voltage source model is shown on the figure 5.2d.

Conclusion

Voltage source model cannot be used for modelling vibration harvesting module because it does not reflect output characteristics of the module: in the observed data very low power output is registered on the low resistance load range whereas in voltage source model power output is the highest at very low values of the load. However, there are certain similarities: voltage output and power output in the high resistance range are similar to the ones observed during the experiment.
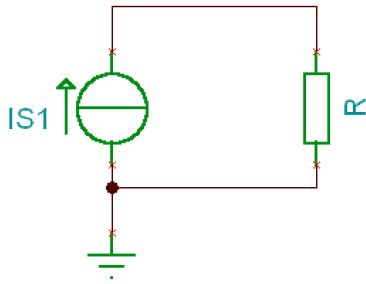
Current source

Next model is the current source model. It is an ideal component which is supplying constant current without any relationship to the load.
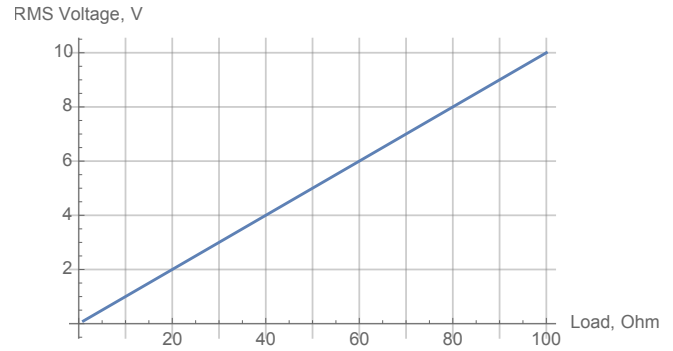
Assumed parameters for the current source model are shown in table 5.2. The curve for voltage versus load presented on the figure 5.3b. figure 5.3c shows relationship current output of the circuit as a function of load. Power output curve for the voltage source model is shown on the figure 5.3d.
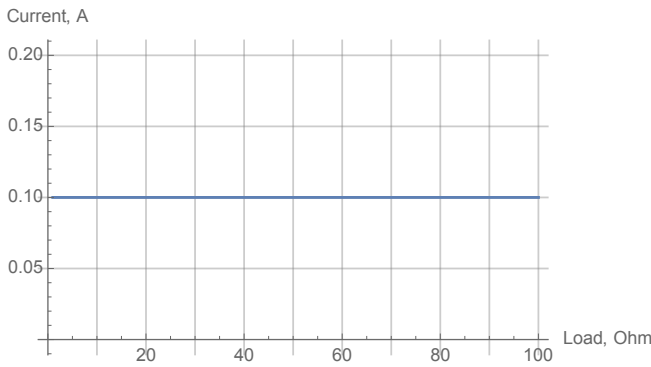
Table 5.2: Current source example parameters

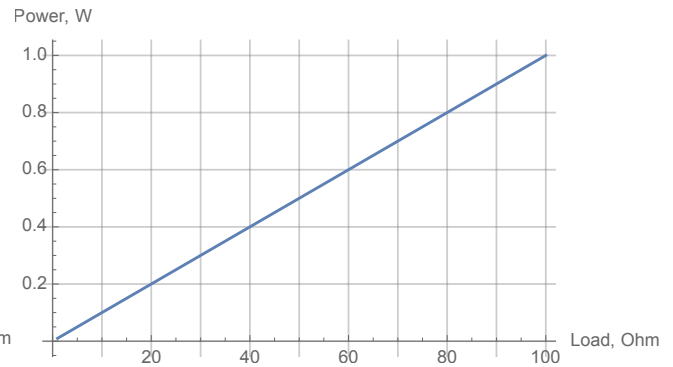| Parameter	Value
IS1, A	0.1

(a) Current source model curcuit

(b) Voltage output

(c) Current output

(d) Power output

Figure 5.3: Current source model figures

Conclusion

Current source model does not fit the observed data: power output plot is linear whereas in the observed data power output plot has non-linear characteristic.

Thevenin's equivalent

In this subsection Thevenin's equivalent will be studied. It is a modification of the voltage source model with so-called 'internal resistance'. The circuit is shown in the figure 5.4a.

Parameters of the following model are written in table 5.3. The curve for voltage versus load presented on the figure 5.4b. figure 5.4c shows current output of the circuit as a function of load.
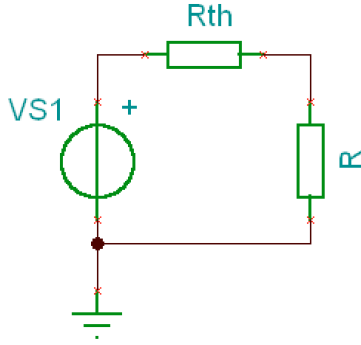
Power output curve for the voltage source model is shown on the figure 5.4d.
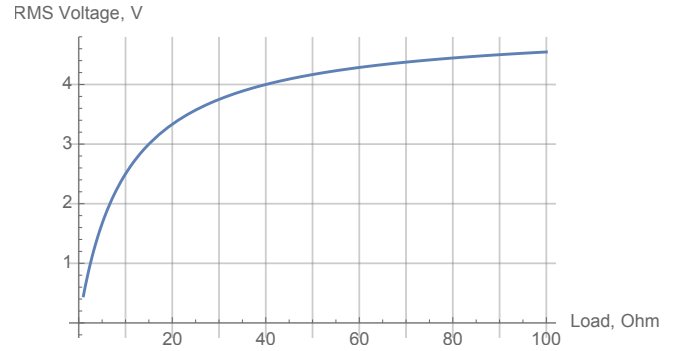
Conclusion

In the figures presented below it is visible that Thevenin's equivalent model can be a good
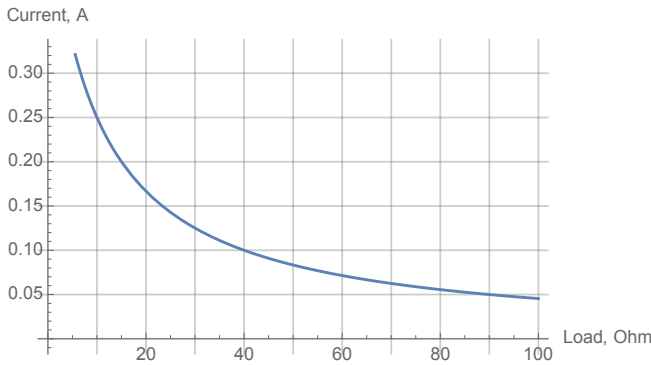
Table 5.3: Thevenin's equivalent example parameters

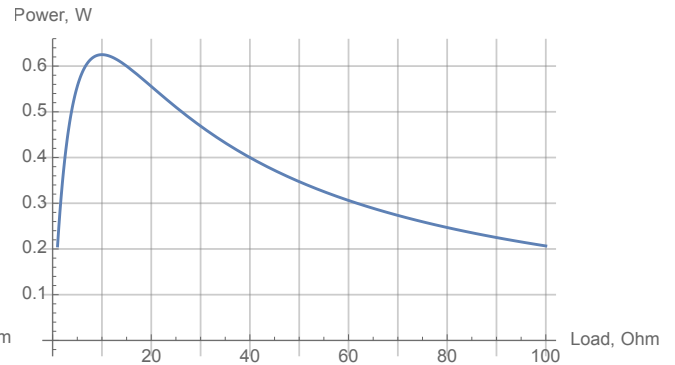| Parameter	Value
VS1, V	5
Rth, Ω	10

(a) Thevenin's equivalent circuit

(b) Voltage output

(c) Current output

(d) Power output

Figure 5.4: Thevenin's equivalent model figures

candidate for mathematical representation of the piezoelectric module. Further the model is fitted to the observed data. In addition it is necessary to check whether the internal resistance is constant or it is changing.

5.3.2 Internal resistance

$$I_{circuit} = \frac{V_{\text{th}}}{R_{\text{load}} + R_{\text{internal}}} \tag{5.3}$$

$$R_{\text{internal}} = \frac{V_{\text{th}}}{I_{\text{circuit}}} - R_{\text{load}} \tag{5.4}$$

In these calculations it is assumed that Thevenin's voltage V_{th} is equal to open-circuit voltage $V_{\text{open-circuit}}$. The obtained results show that internal resistance is not constant and can be

approximated successfully by using linear relationship shown in equation (5.5).

$$R_{\text{internal}} = R_{\text{internal}}(I_{circuit}) = a \times I_{circuit} + b \tag{5.5}$$

where a and b are constant coefficients.

Figure 5.5 (X stands for internal resistance $R_{internal}$) shows calculated internal resistance and its linear approximation. The coefficient of determination R^2 for resonance case is equal to 0.969 (the closer to 1.0 the better fit).

Data for all the studied cases is shown in the table 5.4. In all the cases, except for 140 Hz, a very good correlation was observed. In the case of 140 Hz no correlation between internal resistance and current was observed, i.e. relationship seemed to be almost random. It is important to state that this frequency is more than two times higher than the resonance frequency, therefore an instability in piezoelectric material could be observed. In the reverse process (generation of mechanical oscillations by applying AC) even harmonics cannot induce charges of opposite sign at the two crystal surfaces, therefore no oscillations or unstable oscillations is observed. The same effect can be seen in this case.

According to the obtained values of the a coefficient, the minimum value (internal resistance is less dependent on current) is at the resonant frequency. On the higher frequencies a is growing, and near the second harmonic it is suddenly significantly decreasing its value. However, the data for second harmonic is not reliable and therefore no conclusion regarding drop of the coefficient a can be made. This issue should be further addressed in separate studies.

No dependency of coefficient b on any parameters was observed as it seems to be random. Value of the b is low comparing to load resistance, therefore it can be approximated to zero. The observed fluctuations can be explained by insufficient precision of the testing method used. More detailed research on internal resistance of the piezoelectric module should be conducted.

5.3.3   Power output

Another important aspect in the provided experiment is power output of the harvesting module. By using linear varying model of the internal resistance described above, power output was calculated and compered to the observed data. Good correlation was observed. However, according to maximum power transfer theorem the peak in power output shall be at the point when the load resistance is equal to the internal resistance. In spite of the accurate output power estimation, internal resistance did not match the estimated value (almost two times higher). Therefore, two Thevenin's models with constant internal resistance are compared for power output fitting: the first one where Thevenin's voltage is equal to open-circuit voltage, and the second one with fitted voltage parameter.

Microsoft Excel Solver add-in is used for fitting the model. This add-in is manipulating
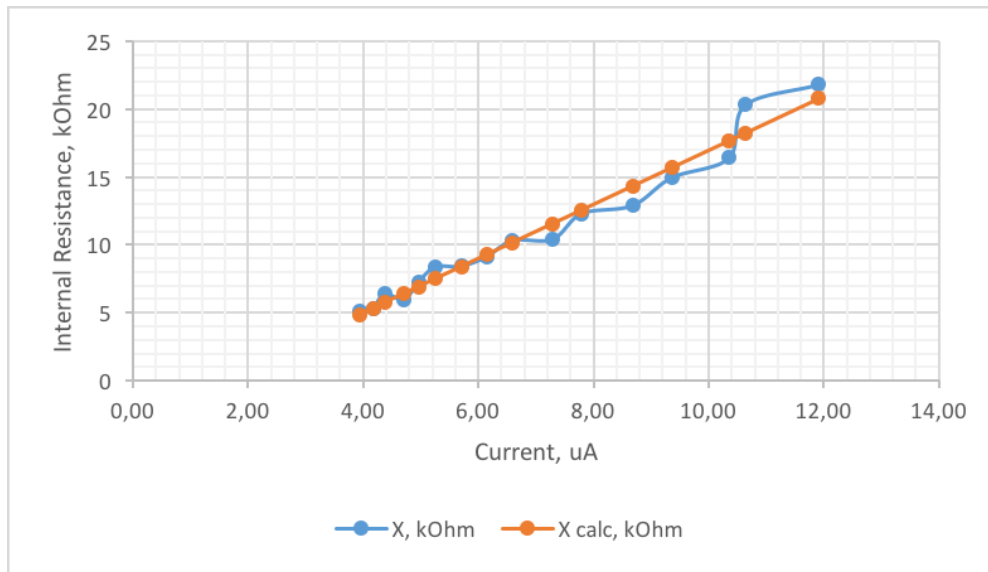
Figure 5.5: Calculated internal resistance and its linear approximation

Table 5.4: Linear approximation of the internal resistance of the piezoelectric module

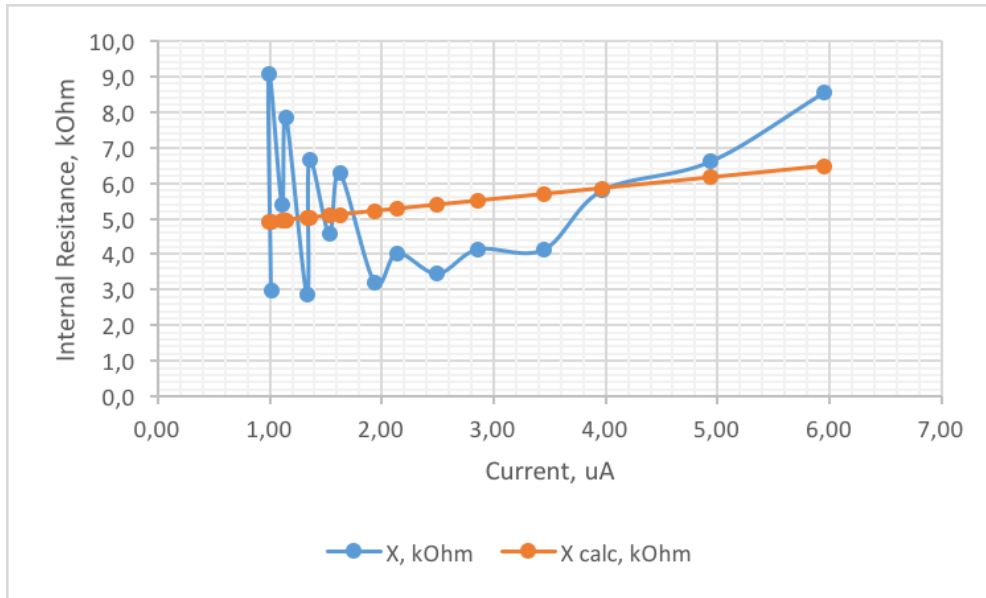| $R_{\text{internal}} = a \times I_{\text{circuit}} + b$				
f,	$V_{\text{op.c.}}$,	a,	b,	R^2
Hz	mV	$\text{k}\Omega\,\mu\text{A}^{-1}$	$\text{k}\Omega$	–
61	316	2,00	-3,04	0,969
65	168	3,24	-1,14	0,954
70	102	5,14	-2,69	0,926
75	80	5,38	-3,91	0,840
81	76	2,70	1,75	0,890
88	52	6,48	-5,23	0,958
120	22	7,47	-0,95	0,965
140	79	0,32	-4,59	**0,056**

Figure 5.6: Attempt of linear approximation of internal resistance $140\,\mathrm{Hz}$ case

variable cells within specified limit in order to minimise or maximise the target cell value. Spreadsheet should have the form shown in table 5.5. Where 'P observed' is the observed value from the experiment, and 'P calculated' is the calculated value using Thevenin's equivalent.

In order to perform the fitting of the model it is important to estimate how accurate is the model's prediction, i.e. how significant is the error when applying the model. This is done by calculations of Residual Sum Of Squares (RSS). It is defined as shown in equation (5.6). The formula provides an accurate estimate for error because it ignores the sign of error by taking a square of the difference, such that the errors of approximately the same absolute value but opposite signs will not cancel each other.

$$RSS = \sum_{i=1}^{n} (y_i - f(x_i))^2 \tag{5.6}$$

Table 5.5: Spreadsheet form for the model fitting analysis

R, kΩ	P observed, mW	P calculated, mW
10	0,1	0,3
12	0,2	0,3
...	...	...

Variables for the following case are: Vth and Rth. The only restriction they have is that both values should be positive. Default GRG nonlinear solver is used. Solver window is showed in figure A.3.

By using the described method the parameters of the Thevenin's equivalent model are estimated. After fitting the data to the model the resultant V_{th} is way higher than measured open-circuit voltage. Internal resistance for Thevenin's equivalent is calculated as shown in the equation (5.4).

Because of non-linearity of power output, data fitting cannot be checked by using conventional R^2 coefficient used above, instead graphical comparison of residuals is used. This method obviously shows the best model for power output approximation. Figure 5.7 shows residuals for the following cases: non-linear resistance model ('non-lin res'), constant resistance model with open-circuit voltage ('Const res'), constant resistance model with fitted voltage ('Thevenin').
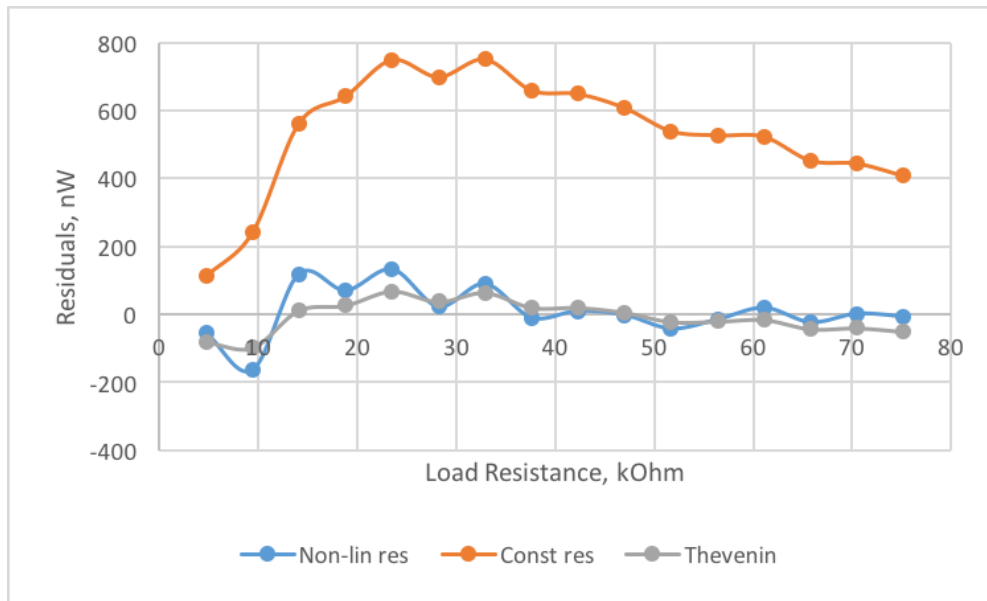

Figure 5.7: Power output residuals for 61 Hz resonance case

Comparison between the estimates, calculated using the described models and the observed data is shown in the figure 5.8. In this figure the following labels for data series are used: 'P' is observed data, 'Pch' is non-linear resistance model, 'Pco' is constant resistance model with open-circuit voltage, and 'Pth' is constant resistance model with fitted voltage.

Table 5.6 and table 5.7 shows calculated power output for different frequencies for both motors as well as internal resistance according to maximum power transfer theorem.

5.4   Natural oscillations test

For the purpose of estimation of the resonance frequency, method described in [16] was used. This method can provide accurate results of dynamic response of the piezoelectric module as an electrical-mechanical resonance system, such as: resonance frequency, damping factor and Q-factor. These characteristics are unique to each testing setup and in case of any changes in mechanical design or conditions this test should be repeated in order to ensure if the parameters are still the same or alternatively to obtain new values of the parameters.

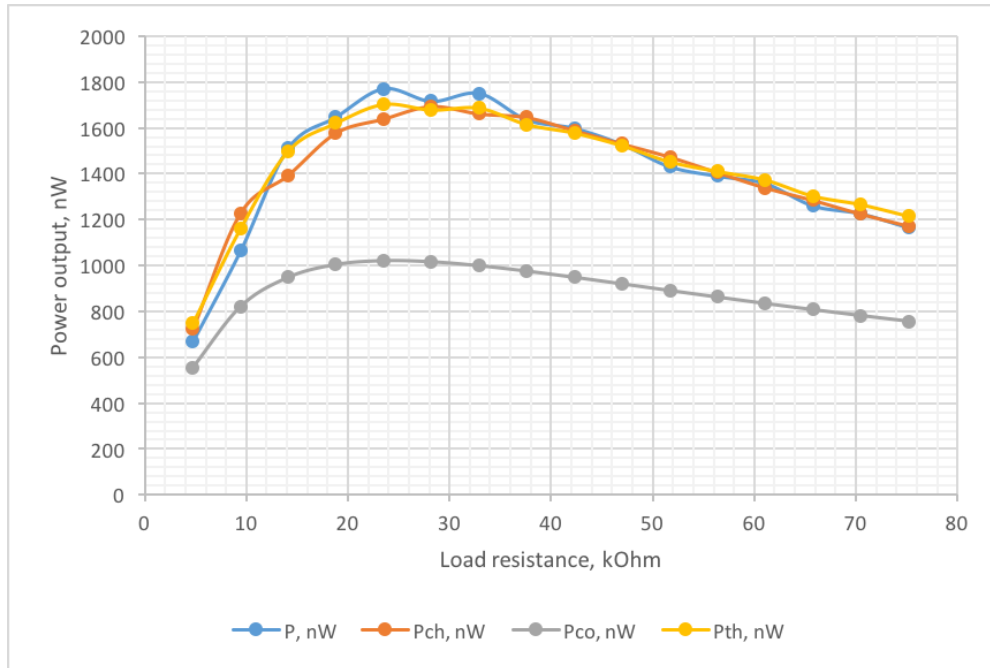Waveform of the natural oscillations are shown in figure 5.9. Observed oscillations are so-

Figure 5.8: Power output for 61 Hz resonance case

Table 5.6: Power output calculations results for 1st vibration motor

f, Hz	R_{int}, kΩ	Max amplitude, mV	Max power, nW
61	24,41	316	1771
65	24,43	168	515
70	23,81	102	211
75	23,46	80	161
81	21,84	76	141
88	17,51	52,4	77
120	12,96	22	15
140	16,59	79	223

Table 5.7: Power output calculations results for 1st vibration motor

f, Hz	R_{int}, kΩ	Max amplitude, mV	Max power, nW
52	46,65	142	360
61	32,46	408	3112
72	23,89	130	376
78	18,74	88	232
83	25,1	72	133
87	23	62	115
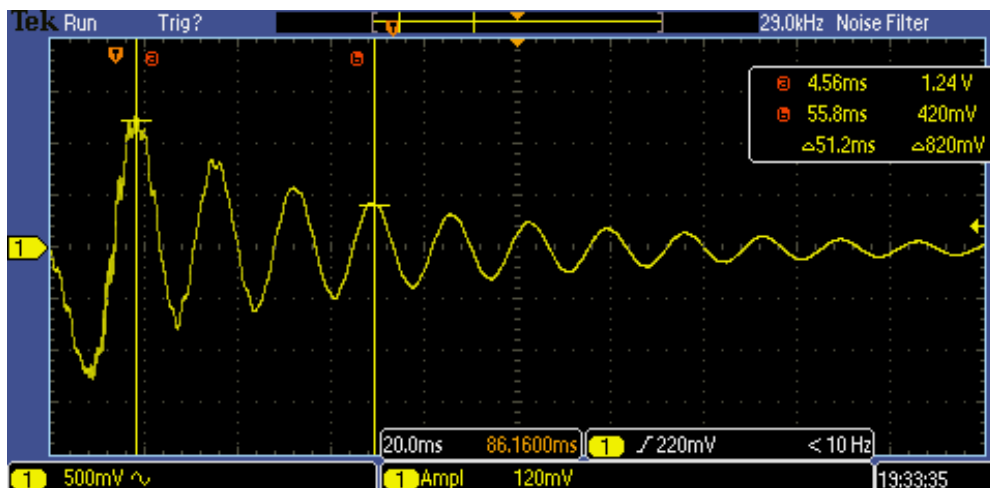
Figure 5.9: 3rd natural oscillations test

called damped oscillations. As it can be seen in the figure, three periods of natural oscillations are about $3 \times T_{\mathrm{nat}} = 51.2 \, \mathrm{ms}$. Natural frequency can be calculated as shown if equation (5.7).

$$f_{\mathrm{nat}} = \frac{3}{3 \times T_{\mathrm{nat}}} = \frac{3}{51.2 \, \mathrm{ms}} = 58.6 \, \mathrm{Hz} \tag{5.7}$$

The obtained result is quite close to the experimentally discovered resonance point. Unfortunately, with the current testing setup it is not possible to make measurements at this particular frequency or at the lower frequency.

In order to find damping factor and Q-factor for the system, peaks of the waveform needed to be digitised. Additional issue represents the fact that peaks are biased, i.e. mean value of two neighbour peaks is not 0, so values are needed to be normalised. Bias measurement and fitted second order estimation are shown in the figure 5.10 for the second natural oscillations test. It is visible that estimation is quite accurate. Normalised absolute values of the peaks for the 2nd natural oscillations test are shown in the table 5.8.

According to the theory of under-damped oscillations, absolute values of the peaks should follow equation (5.8).

$$V = a \times \exp\left[-\gamma \times (t - t_0)\right] \tag{5.8}$$

where:

a = is the theoretical amplitude of the first oscillation, [mV]

γ = is the decay rate [s^{-1}]

t_0 = is the time when oscillations are starting [s]

By using Microsoft Excel's Solver exponential model was fitted to the absolute value of the peaks. The result is shown in the figure 5.11. The same method was used for all three natural oscillations tests.

The damping coefficient ζ is found as shown in equation (5.9).

$$\zeta = \frac{\gamma}{\omega_0} \tag{5.9}$$

where ω_0 is the natural angular frequency.

Natural frequency of oscillations is different from the damped oscillations frequency and can be found as shown in equation (5.10). Natural frequency in the current case can be assumed to be the same as the observed frequency of the oscillations due to γ being about $15 \, \mathrm{s}^{-1}$ while ω is approximately equals to $2\pi f = 2\pi \times 60 \, \mathrm{Hz} = 377 \, \mathrm{s}^{-1}$, therefore change in angular frequency is negligible. It is shown in equation (5.11).
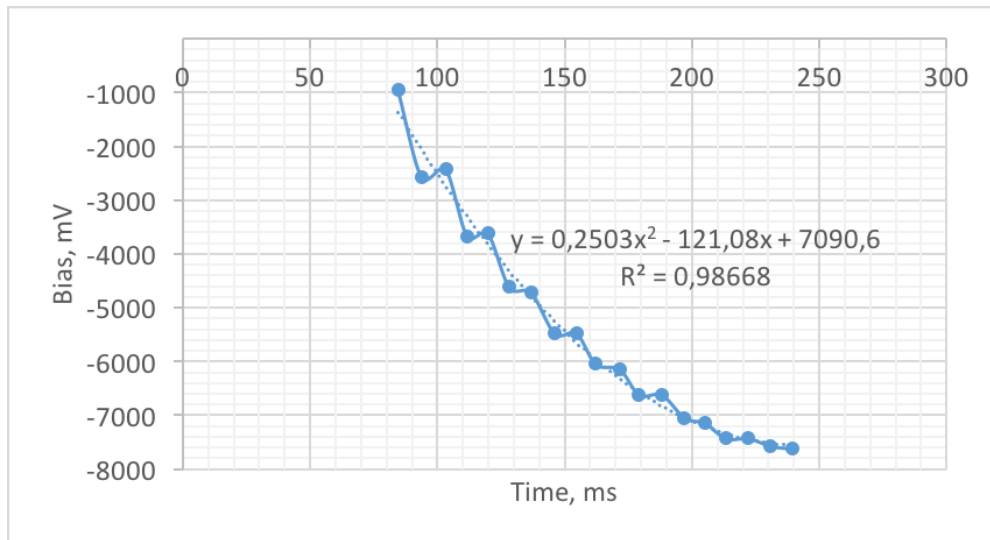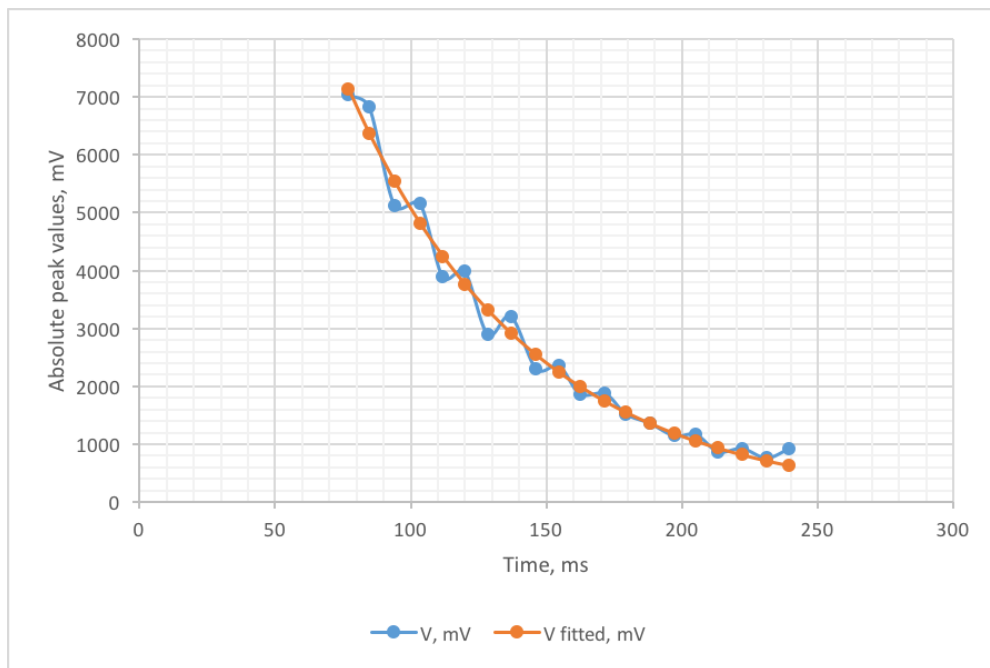
Figure 5.10: Bias measurement and fitted estimation

Figure 5.11: Absolute values of peaks and fitted estimation

Table 5.8: Positive peaks of natural oscillation waveform

#	t, ms	V, mV	#	t, ms	V, mV
1	77,0	7037	11	162,3	1871
2	84,7	6824	12	171,6	1874
3	94,0	5127	13	179,2	1523
4	103,3	5157	14	188,1	1360
5	111,8	3890	15	197,0	1145
6	119,9	3983	16	205,1	1166
7	128,3	2898	17	213,1	871
8	136,8	3209	18	222,0	926
9	146,1	2307	19	231,0	762
10	154,6	2352	20	239,4	924

$$\omega_0 = \sqrt{\omega^2 + \gamma^2} = \sqrt{(2\pi f)^2 + \gamma^2} \tag{5.10}$$

$$\omega_0 = \sqrt{377^2 + 15^2} = 377.3\,\mathrm{s}^{-1} \approx 377\,\mathrm{s}^{-1} \tag{5.11}$$

Q-factor is found using equation (5.12).

$$Q = \frac{1}{2\zeta} \tag{5.12}$$

Calculated values of the amplitude a, natural frequency f, damping coefficient ζ, Q-factor Q for all 3 test are shown in table 5.9.

Table 5.9: Natural oscillations test results

#	a, V	f, Hz	ζ	Q
1	1,716	59,9	0,0396	12,6
2	18,87	59,5	0,0416	12,0
3	15,71	58,9	0,0450	11,1
	Average	59,4	0,0421	11,9

5.5   Effective range of operation

Q-factor can be used to describe effective range of operations. It is very useful in current case because this factor is characterising bandwidth according to energy output: bandwidth over which the power of vibration is greater than half the power at the resonant frequency is equal to $f_0 \pm \Delta f$ [7]. Where Δf is calculated as shown in equation (5.13).

$$\Delta f = \frac{f_0}{Q} \tag{5.13}$$

In natural oscillations test values of $f_0 = 59.4 \, \text{Hz}$ and $Q = 11.9$ were obtained, therefore for the current setup effective frequency range is $59.4 \pm 59.4/11.9 \, \text{Hz} = 54.4 \, \text{Hz}$ to $64.4 \, \text{Hz}$.

This result fits behaviour of the system in power output tests: at frequency of $61 \, \text{Hz}$ (near resonance) power output is $1771 \, \text{nW}$, while at $65 \, \text{Hz}$ power output is down to $515 \, \text{nW}$, which is more than three times less. Therefore, the conclusion can be made that natural oscillations test is enough to determine effective range of operation of the module.

5.6   Second vibration motor test

In this section results obtained while testing the second vibration motor are being discussed. In general, all the data which was acquired using the first vibration motor was confirmed on the test with the second one, for example purely distinguishable resonance is at nearly the same frequency. Much higher power output was observed due to more powerful characteristics of the motor. However, results on internal resistance or others cannot be taken into consideration without special treatment due to the considerable amount of noise in the signal. Even oscilloscope's built-in noise filtering system was not able to handle the noise. In some cases amount of noise was comparable to waveform itself, therefore obtained results are used only for quantitive analysis.

Chapter 6

Conclusion

6.1 Summary

In this thesis possible application of vibration harvesting modules in subsea wells were studied and discussed. It was concluded that natural oscillations test can give such important characteristics of the system as resonance frequency and Q-factor. By using these parameters the effective range of the vibration harvesting module can be estimated. Information concerning internal resistance and power output can be obtained only by testing, as it was demonstrated. Extremely low power output levels were achieved due to the operation of the vibration motors in a low vibration mode. This was done intentionally in order to produce vibrations of the desired frequencies. Resonance frequency and effective operation range were obtained by two different tests and results of those tests were comparatively similar. It has been demonstrated that while Thevenin's equivalent can quite accurately describe power output characteristics this mathematical model fails to describe internal resistance due to its dependency of on a current. Many other factors should be studied in order to properly describe both power output and internal resistance using the same model.

All the identified research questions were addressed and answered. Brief answers are given below.

Question 1: response is AC with frequency equal to the vibration frequency. Further details are provided in section 5.1.

Question 2: no unite model was obtained, however power output is well described by Thevenin's equivalent with constant internal resistance, while internal resistance is accurately described by Thevenin's equivalent with internal resistance linearly dependent on current. Further details are provided in section 5.3.

Question 3: the maximum achieved power output was $3.1\,\mu W$ which is extremely low. Values up to milli watts could be achieved according to the [16].

Question 4: for the current module effective operating range was estimated from $54.4\,Hz$ to $64.4\,Hz$. Estimate was based on natural oscillation test and was confirmed by another test. Further details are provided in section 5.5.

6.2 Further suggestions

The assumption which assumes linear relationship between supplied electric energy and vibration energy emitted should be studied further. This assumption does not need necessarily

be true in certain cases, due to possible resonance characteristics and non-linear relationship for efficiency of the motors.

Quite narrow range of vibrations was generated during the experiment. For more detailed research the use of closed-loop electromagnetic shaker as a source of vibrations instead of vibration motors can be suggested, as it allows to produce vibrations with known characteristics: displacement, velocity, and acceleration. This device can help to gather much more specific information related to vibrations being tested including energetic characteristics. In order to provide even more accurate data special equipment such as laser measuring devices is suggested to be used to verify and to define more precisely foregoing characteristics.

In terms of clamping of the piezoelectric module it is recommended for the further research to use specially designed `PPA-5001` clamp base. It can potentially provide an easier way to fix the module and make test more precise and accurate.

Appendices

Appendix A

Additional information

A.1 Breadboard vs Printed Circuit Board (PCB)

In this section some additional information about breadboards and PCB is provided. Typical breadboard is shown on the Figure A.1, and its layout is shown on the Figure A.2 below.
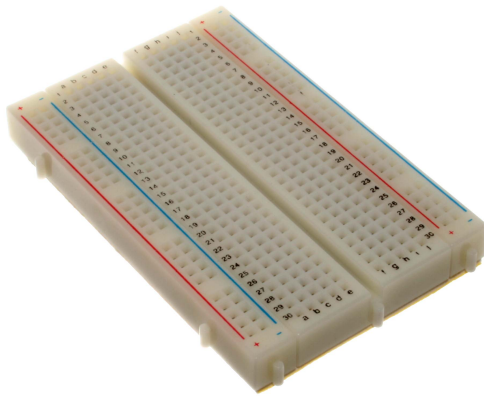
Figure A.1: Typical breadboard
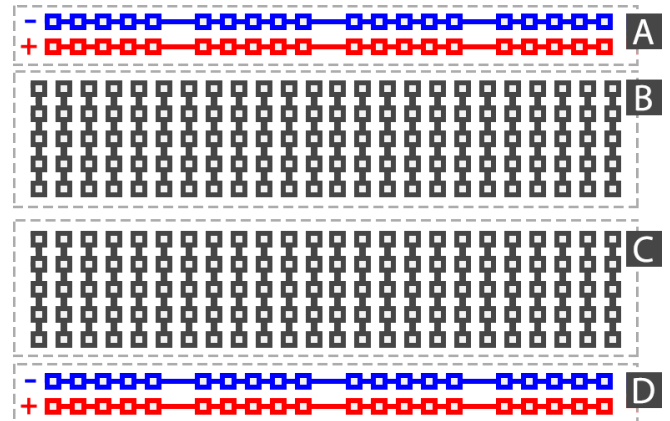
Figure A.2: Typical breadboard layout

Breadboard itself provides a convenient way for fast prototyping of electronic circuits. It does not require soldering to make electric contacts between elements, instead it is using metal spring clips to fix wires. Spring clips are situated inside the holes, each hole is connected in groups (usually lines) as shown on Figure A.2. Typical distance between holes is 2.54 mm which is the standard pin's spacing for IC in Dual In-line Package (DIP) packages and for discrete semiconductors in through-hole packages like TO-220. Because of these features breadboards are widely used in designing electronics. Although it is not possible to construct fast operating devices (due to parasitic inductances and capacitance of connecting wires), power devices (due to limitation on current for the conducting tracks) nor high voltage devices (due to isolation limitations). Also it is not possible to use SMD components because of using different technology for fixing and connecting components (surface mounting versus through-hole mounting).

A.2 Addition figures
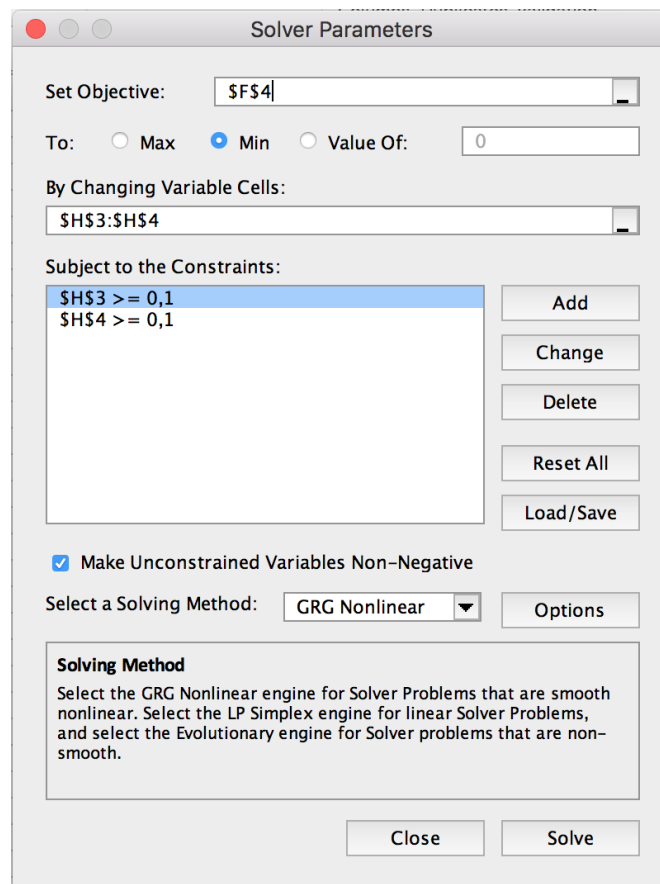
Figure A.3: Solver window

Appendix B

Waveforms

B.1 First motor test open-circuit waveforms
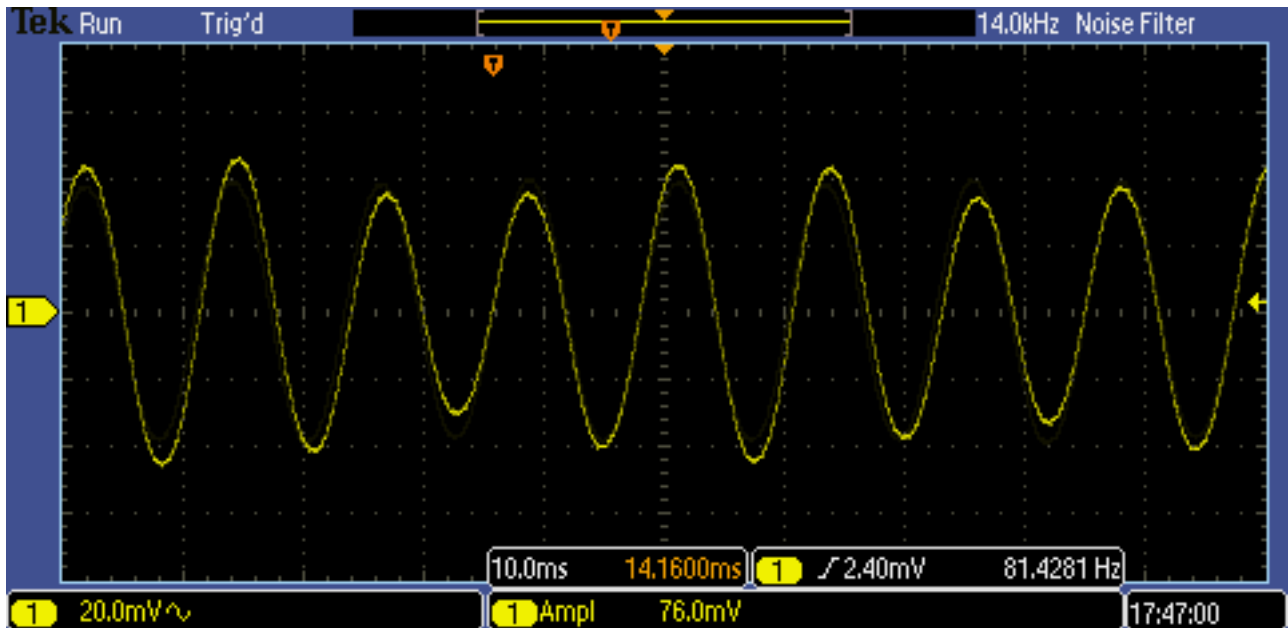
Figure B.1: 61 Hz open-circuit test output waveform
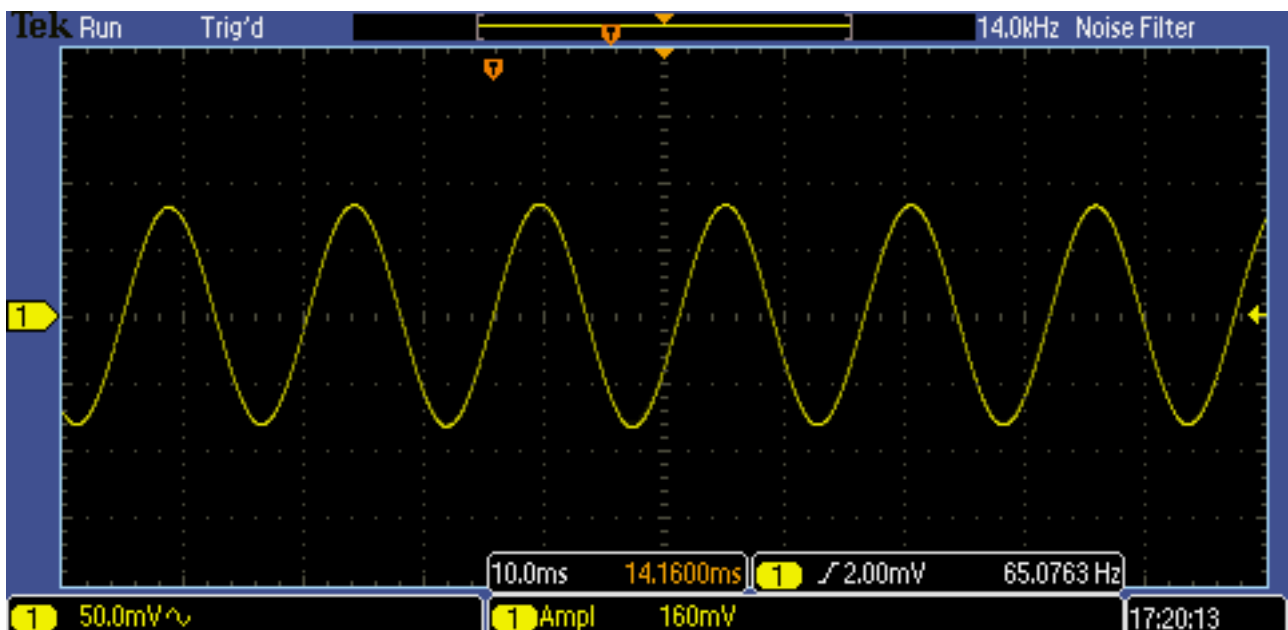
Figure B.2: 65 Hz open-circuit test output waveform
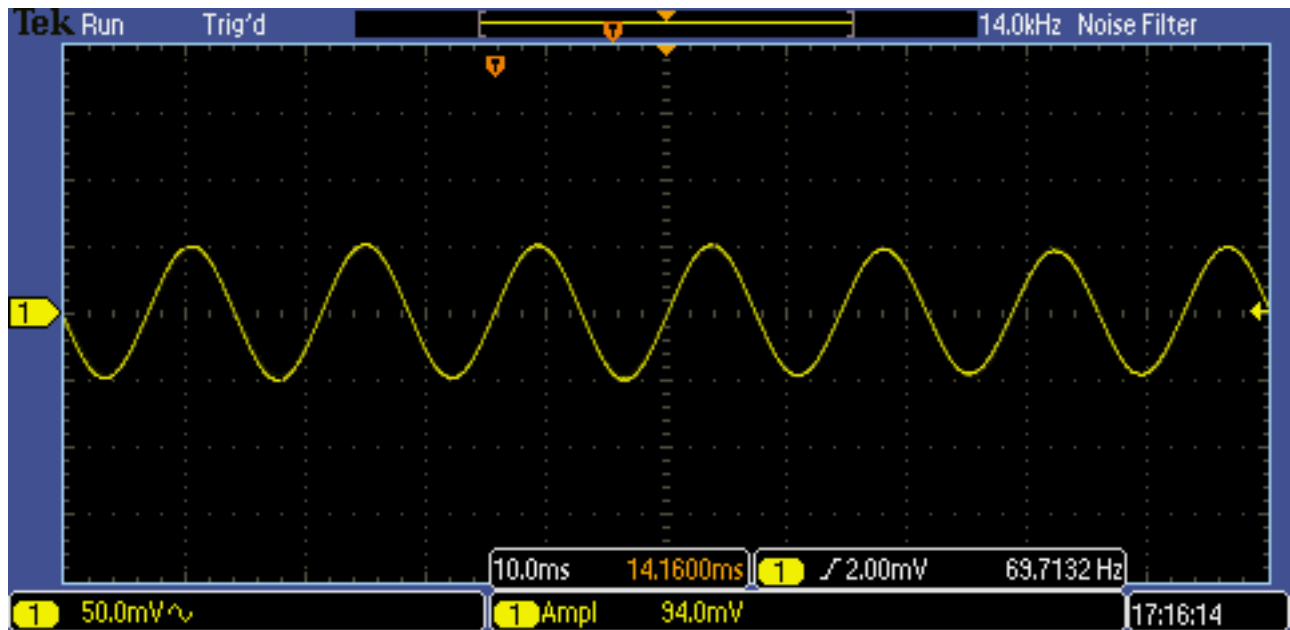
B.2 Second motor test

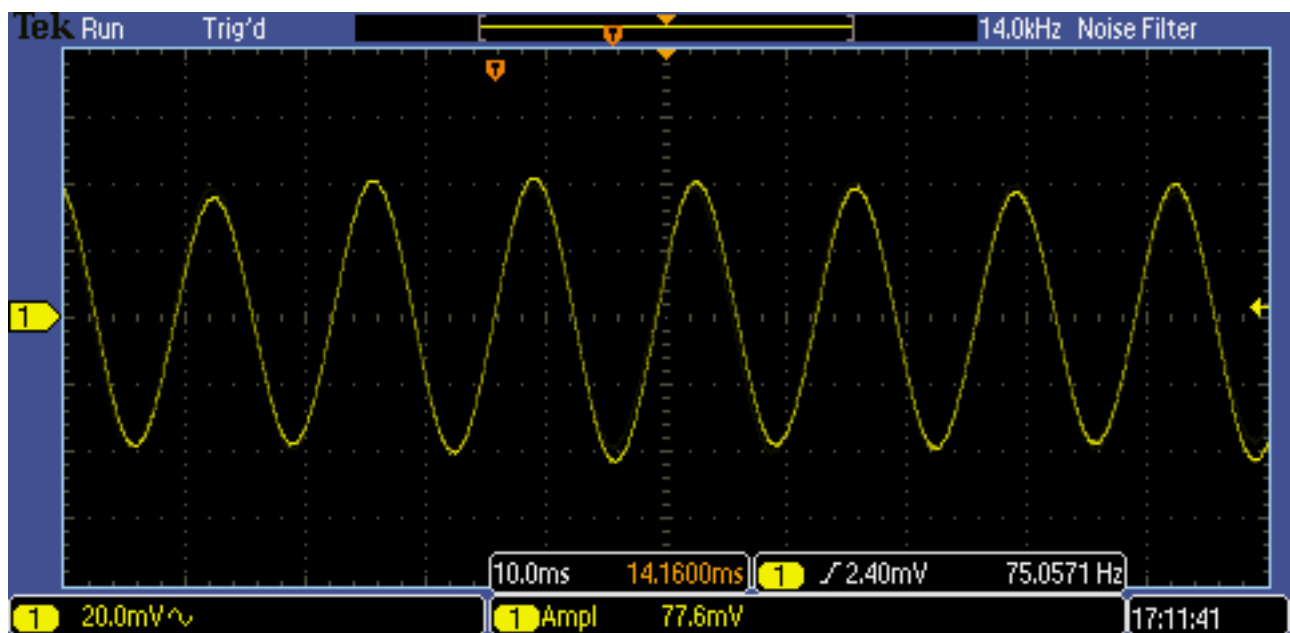Figure B.3: 70 Hz open-circuit test output waveform

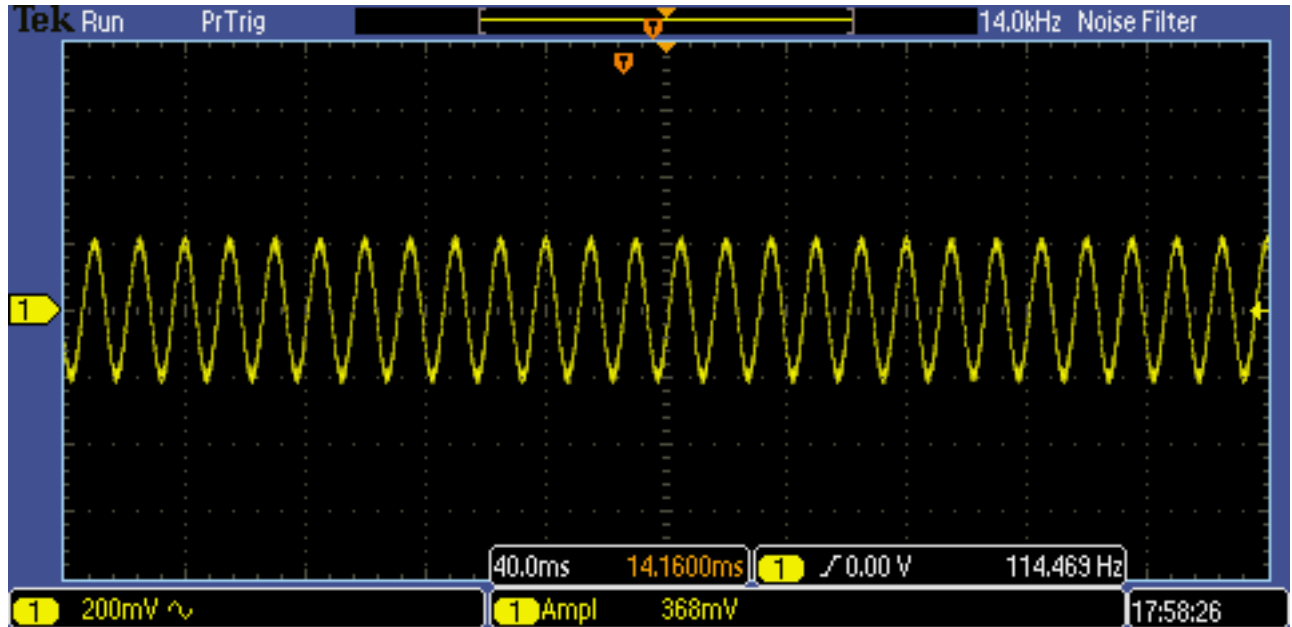Figure B.4: 75 Hz open-circuit test output waveform

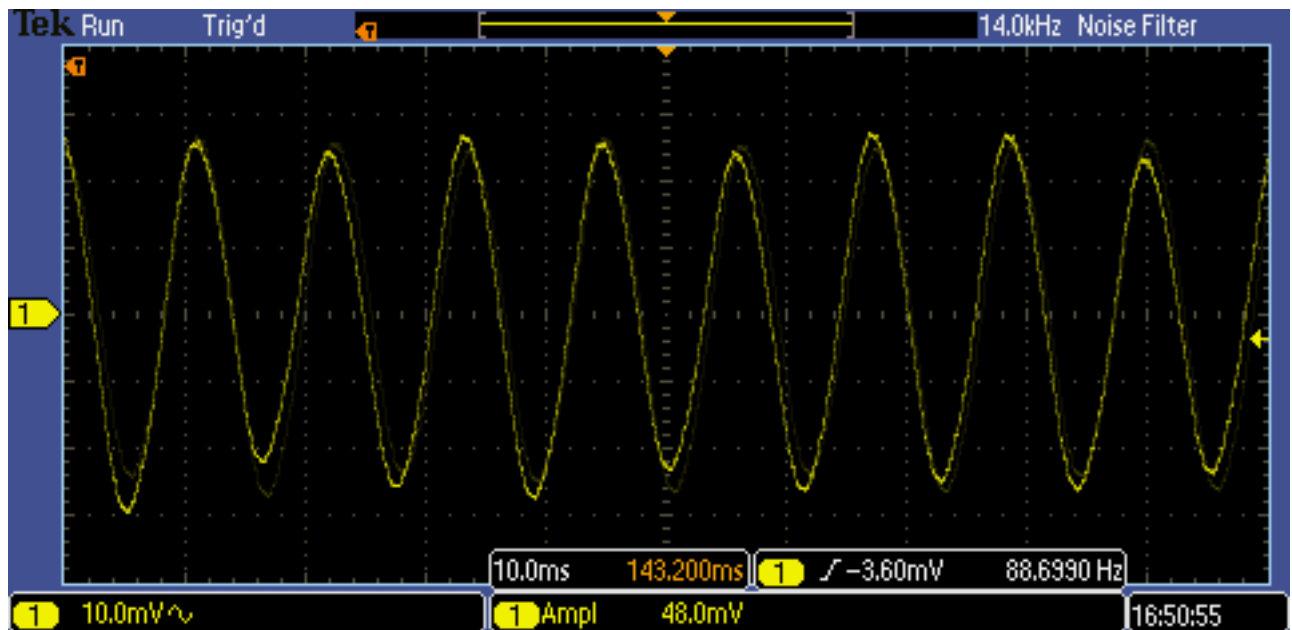Figure B.5: 81 Hz open-circuit test output waveform
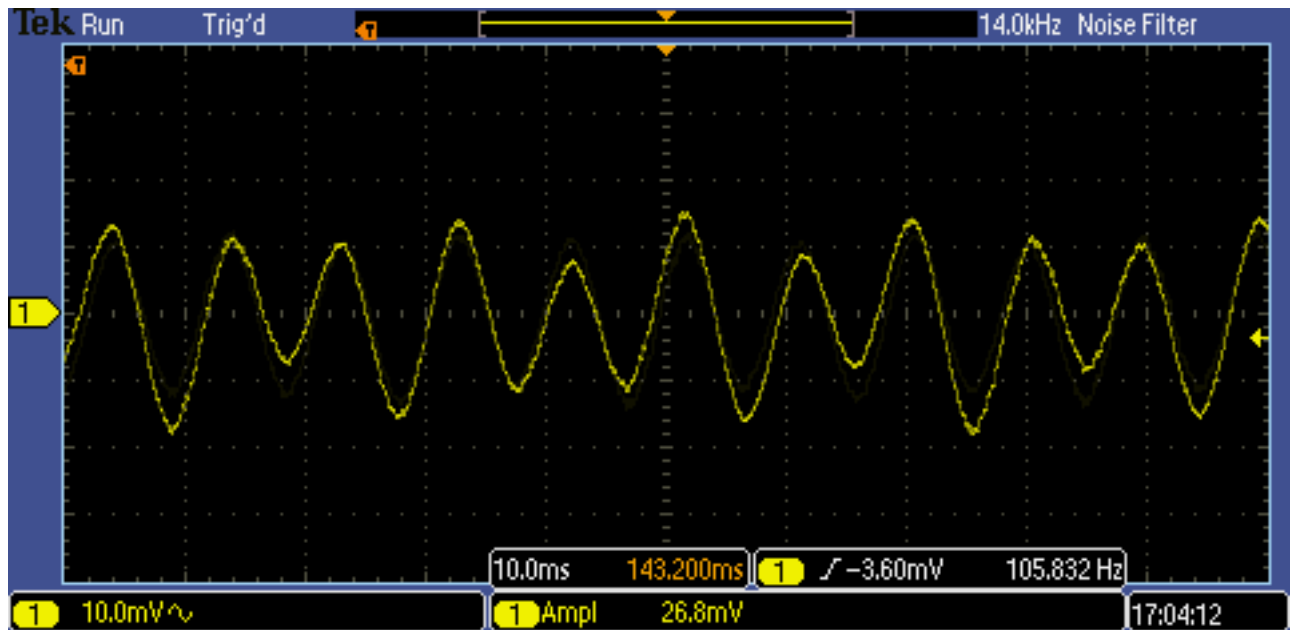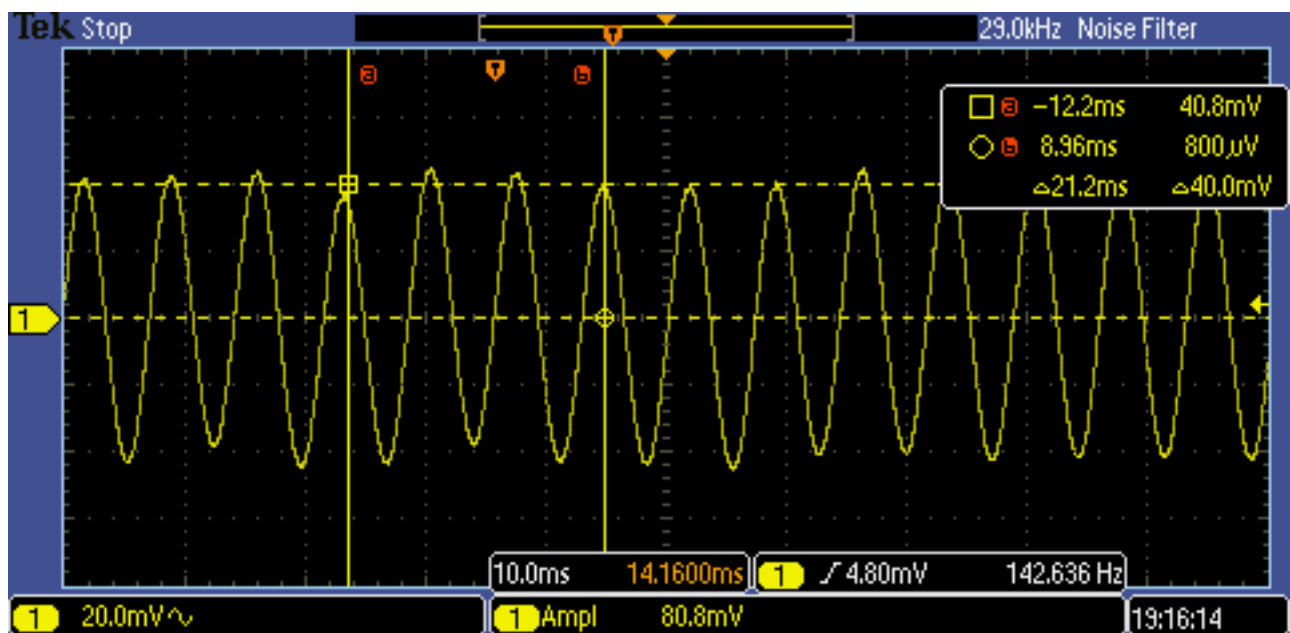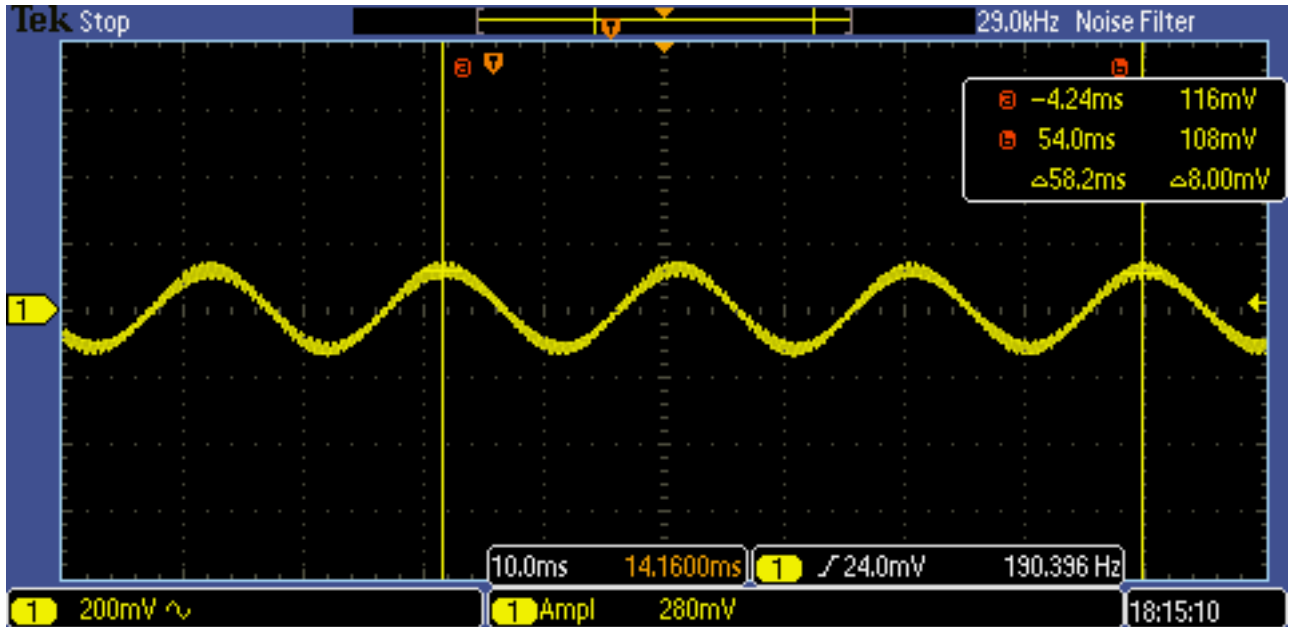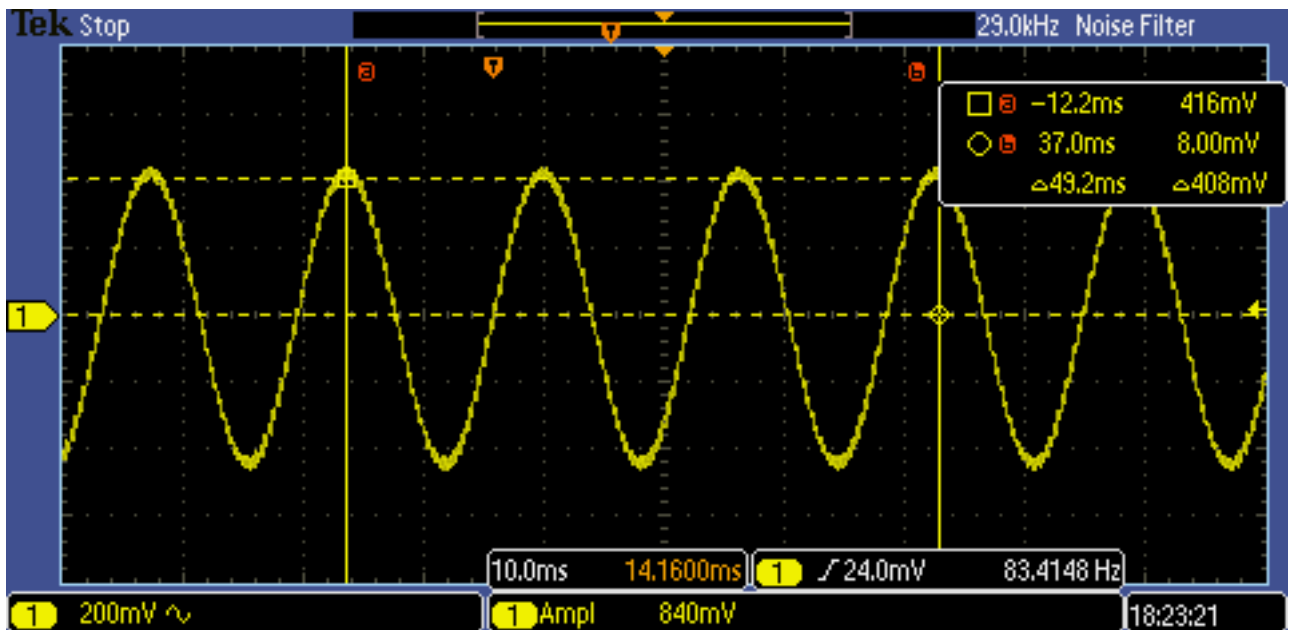

Figure B.6: 88 Hz open-circuit test output waveform

Figure B.7: 120 Hz open-circuit test output waveform

Figure B.8: 140 Hz open-circuit test output waveform

Figure B.9: 52 Hz open-circuit test output waveform

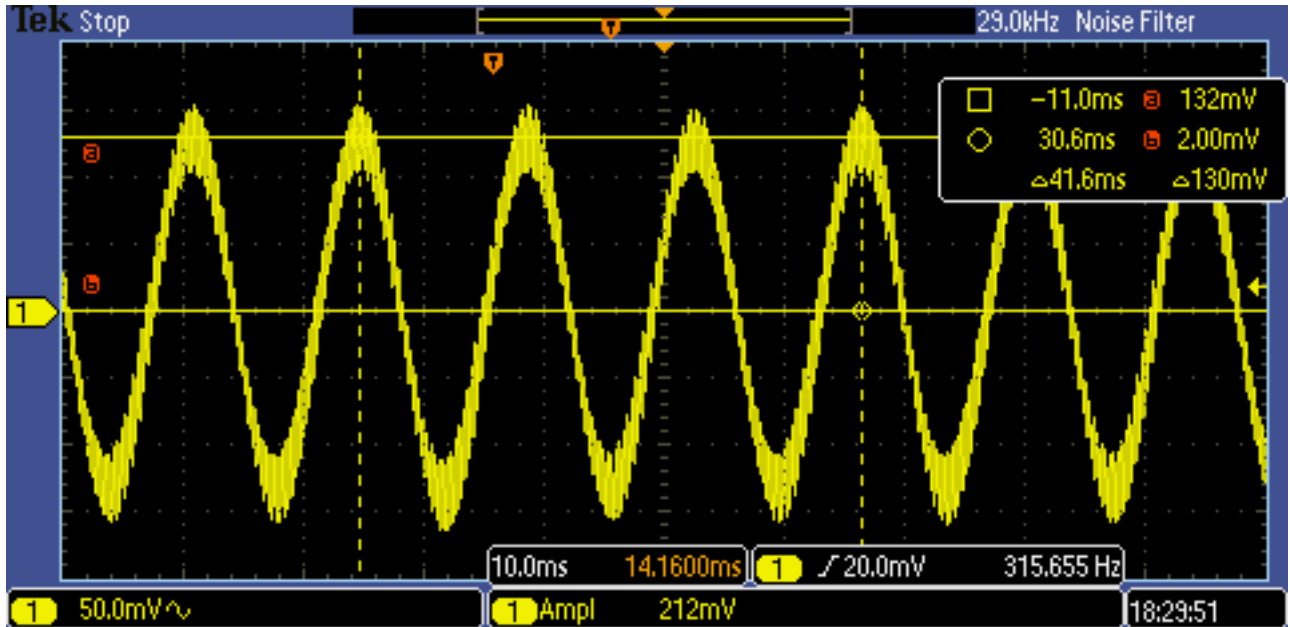
Figure B.10: 61 Hz open-circuit test output waveform

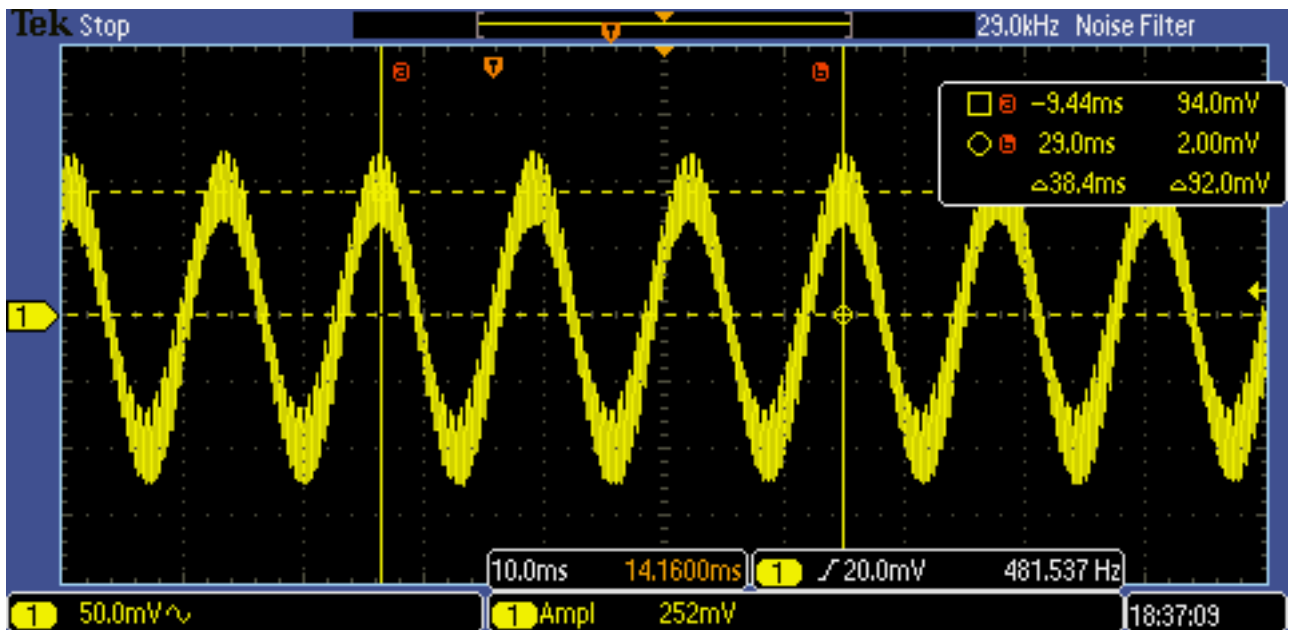Figure B.11: 72 Hz open-circuit test output waveform

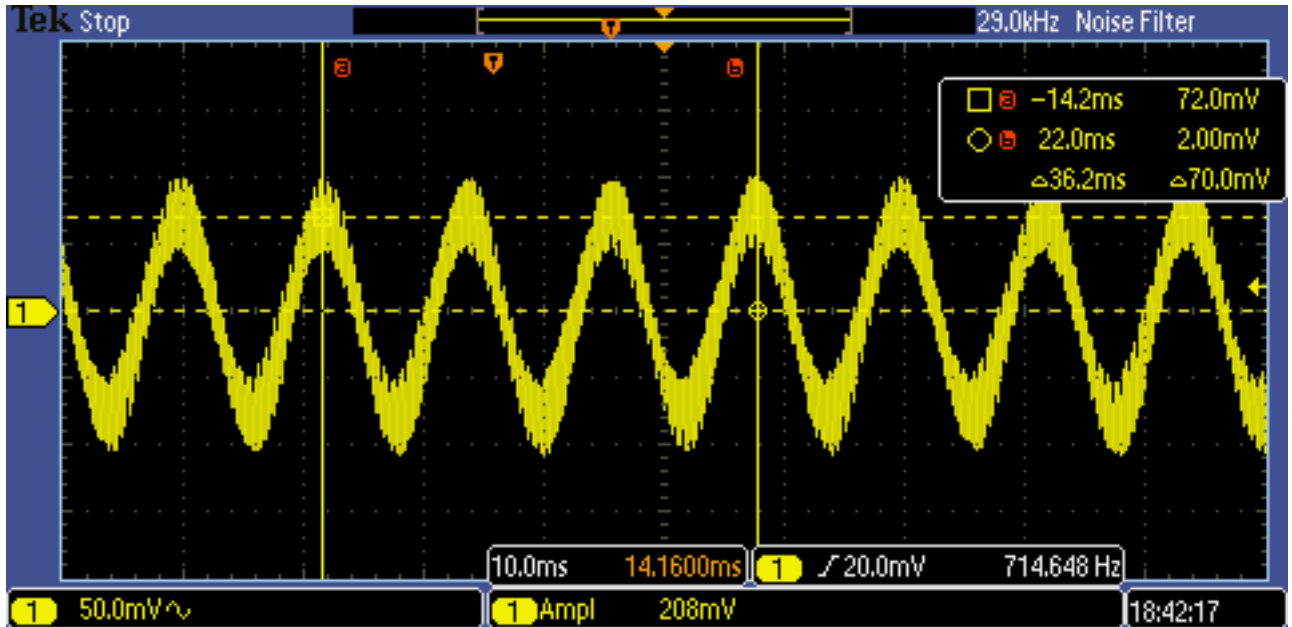Figure B.12: 78 Hz open-circuit test output waveform

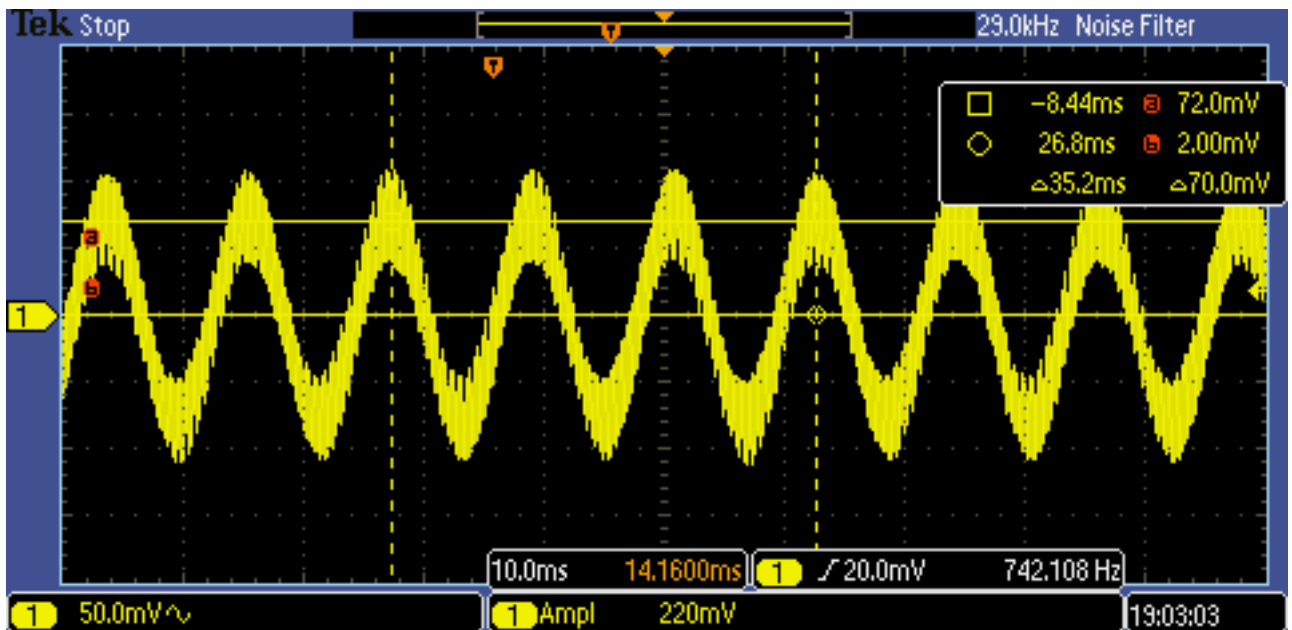Figure B.13: 83 Hz open-circuit test output waveform

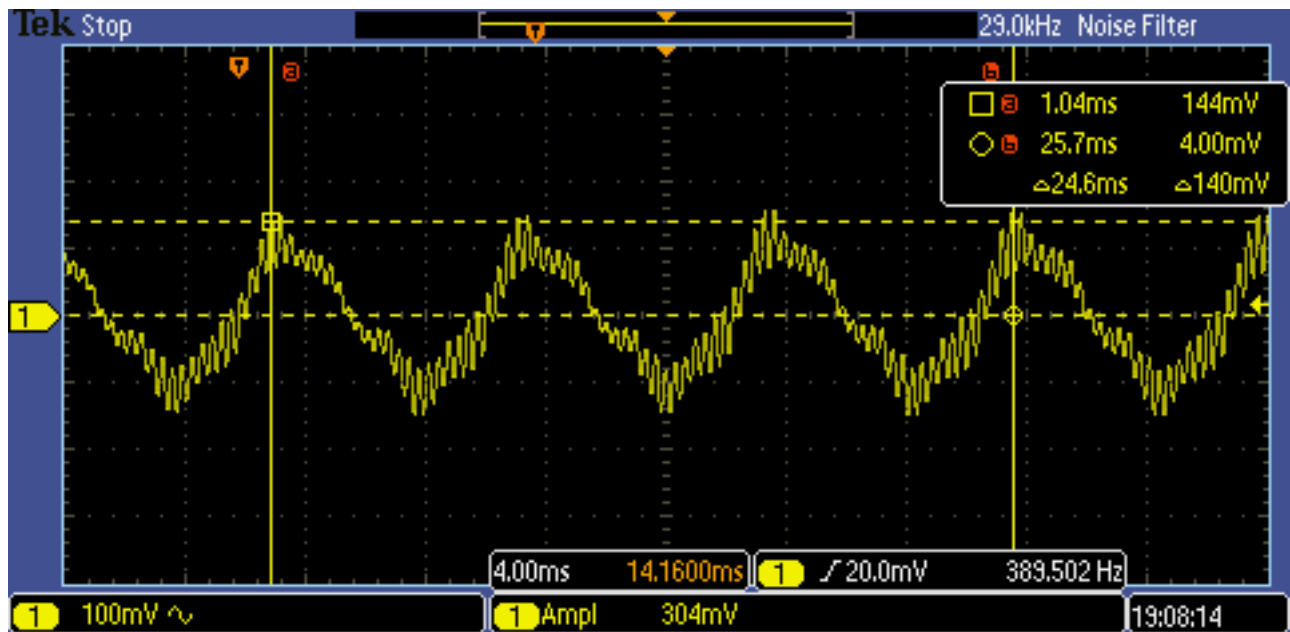Figure B.14: 87 Hz open-circuit test output waveform

Figure B.15: 122 Hz open-circuit test output waveform

Bibliography

[1] API 17D. Specification for design and operation of subsea production systems-subsea wellhead and tree equipment. 2011.

[2] David G. Alciatore. *Introduction to Mechatronics and Measurement Systems (3rd ed.)*. McGraw Hill, 2007.

[3] Terje Baustad. Sub-sea annulus b monitoring. April 2014.

[4] Arduino Community. Arduino uno technical specs. 2016.

[5] NORSOK D-010. Well integrity in drilling and well operations. 2004.

[6] G Gautschi. Piezoelectric sensorics: Force, strain, pressure, acceleration and acoustic emission sensors, materials and amplifiers. 2002.

[7] Paul Horowitz. *The Art of Electronics*. Cambridge University Press, 1989.

[8] Texas Instruments. Lm317 3-terminal adjustable regulator datasheet. 2016.

[9] Vishay Intertechnology. Irl620, sihl620 vishay siliconix power mosfet datasheet. 2011.

[10] Sandia National Laboratories. The science of battery degradation. January 2015.

[11] Kotl JinLong Machinery. C1026b002f (28821) vibration motor datasheet. 2009.

[12] Kotl JinLong Machinery. Z7al2b1692082 (28822) vibration motor datasheet. 2009.

[13] A. Manbachi and Cobbold R.S.C. Development and application of piezoelectric materials for ultrasound generation and detection. 2011.

[14] P Glynne-Jones N M White and S P Beeby. A novel thick-film piezoelectric micro-generator. 2001.

[15] Jean-Baptiste Faget Neil Sultan. Real-time casing annulus pressure monitoring in a subsea hpht exploration well. Technical Report OTC 19286, Total E&P Norge AS, May 2008.

[16] Mide Technology. Ppa products: Datasheet and user manual. 2016.

[17] Ronald E. Walpole. *Probability and Statistics for Engineers and Scientists (9th Edition)*. Prentice Hall, Inc., 2012.

[18] Kyle Wilt. Through wall data and power delivery using ultrasound. May 2015.